



HAL
open science

Transient weakening during the granulite to eclogite transformation within hydrous shear zones (Holsnøy, Norway)

Erwan Bras, Marie Baïssset, Philippe Yamato, Loic Labrousse

► **To cite this version:**

Erwan Bras, Marie Baïssset, Philippe Yamato, Loic Labrousse. Transient weakening during the granulite to eclogite transformation within hydrous shear zones (Holsnøy, Norway). *Tectonophysics*, 2021, 819, pp.229026. 10.1016/j.tecto.2021.229026 . insu-03320760

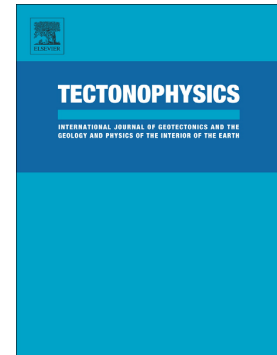
HAL Id: insu-03320760

<https://insu.hal.science/insu-03320760>

Submitted on 16 Aug 2021

HAL is a multi-disciplinary open access archive for the deposit and dissemination of scientific research documents, whether they are published or not. The documents may come from teaching and research institutions in France or abroad, or from public or private research centers.

L'archive ouverte pluridisciplinaire **HAL**, est destinée au dépôt et à la diffusion de documents scientifiques de niveau recherche, publiés ou non, émanant des établissements d'enseignement et de recherche français ou étrangers, des laboratoires publics ou privés.



Transient weakening during the granulite to eclogite transformation within hydrous shear zones (Holsnøy, Norway)

Erwan Bras, Marie Bâisset, Philippe Yamato, Loic Labrousse

PII: S0040-1951(21)00308-5

DOI: <https://doi.org/10.1016/j.tecto.2021.229026>

Reference: TECTO 229026

To appear in: *Tectonophysics*

Received date: 11 March 2021

Revised date: 20 July 2021

Accepted date: 9 August 2021

Please cite this article as: E. Bras, M. Bâisset, P. Yamato, et al., Transient weakening during the granulite to eclogite transformation within hydrous shear zones (Holsnøy, Norway), *Tectonophysics* (2018), <https://doi.org/10.1016/j.tecto.2021.229026>

This is a PDF file of an article that has undergone enhancements after acceptance, such as the addition of a cover page and metadata, and formatting for readability, but it is not yet the definitive version of record. This version will undergo additional copyediting, typesetting and review before it is published in its final form, but we are providing this version to give early visibility of the article. Please note that, during the production process, errors may be discovered which could affect the content, and all legal disclaimers that apply to the journal pertain.

Transient weakening during the granulite to eclogite transformation within hydrous shear zones (Holsnøy, Norway)

Erwan Bras^{a,*} erwan.bras@univ-rennes1.fr, Marie Bâisset^b, Philippe Yamato^{a,c},
Loïc Labrousse^b

^a*Univ Rennes, CNRS, Géosciences Rennes - UMR 6118, F-35000 Rennes, France*

^b*Institut des Sciences de la Terre de Paris, Université Pierre et Marie Curie, 75005 Paris, France.*

^c*Institut Universitaire de France, Paris, France*

*Corresponding author.

Abstract

In Holsnøy (Bergen Arcs, Norway), metastable granulite facies anorthosite rocks are partially eclogitised within hydrous shear zones, that have been interpreted as widening over time with fluid influx and strain. We here present a detailed petrological description of two different metre-scale shear zones from this area. Within a few tens of centimetres of each shear zone, the granulite protolith (initially plagioclase + garnet + two pyroxenes) is transformed into a albite + zoisite + garnet + clinopyroxene assemblage. The outer edge of the shear zones consists in a fine-grained heterogeneous assemblage of omphacite + zoisite + kyanite + garnet + phengite ± albite ± quartz. The core of the shear zones is an homogeneous eclogite assemblage of coarser omphacite + kyanite + garnet + zoisite + phengite ± quartz. As the shear zones widened over time, this lateral evolution from the edge to the core of the shear zones reflects the temporal evolution of the granulite from the beginning to the end of the eclogitisation reaction. The outer omphacite + zoisite + kyanite + garnet + phengite ± albite ± quartz assemblage therefore represents a transient eclogite facies assemblage. Field and petrological observations suggest that this transient assemblage is mechanically weaker than both the starting strong granulite and the final eclogite. We here investigate the impact of transient weakening during syn-tectonic metamorphism using a one-dimensional numerical model of a fluid-fluxed, reacting shear zone. We show that transient weakening is required to explain our field and petrological observations. Furthermore, although the widening of the shear zones was primarily controlled by fluid infiltration, we show that strain

* Corresponding author

hardening during the end of the eclogitisation reactions sequence had a noticeable widening effect on the shear zones.

Keywords

Eclogitization, Metamorphic reactions, Shear zone widening, Transient weakening

1. Introduction

Shear zones are geological features of key importance for understanding the mechanical behaviour of the deep crust (e.g. Fossen and Cavalcante, 2017; Vawemann et al., 2019). The formation and evolution of a deep crustal shear zone is a complex process involving interplay between deformation, metamorphic reaction, fluid and element transport (e.g. Früh-Green, 1994; Austrheim, 1998, 2013; Jamtveit et al., 2016). At large scales metamorphic transformations constitute a first order control on the rheological behaviour throughout the crust. For example, eclogitisation of nominally dry metastable granulite facies has been invoked as a cause for earthquakes in the deep Tibetan crust (Shi et al., 2018). As these large scale processes have only been imaged through geophysical investigations in active orogens (e.g. in the Himalaya, Hetényi et al., 2007), direct petrological and structural observations of exhumed crustal rocks from ancient orogens are crucial in understanding the role of metamorphic reactions on the rheology of the deep crust (e.g. Austrheim, 1990; Jackson et al., 2004; Labrousse et al., 2010).

The island of Holsnøy (Bergen Arcs, Norway) constitutes a natural laboratory for investigating the interplay between eclogitisation, fluid transport and deformation of subducted crust (e.g. Austrheim, 1987, 2013; Putnis et al., 2017; Jamtveit et al., 2019; Zertani et al., 2019). Rocks on Holsnøy are mostly granulite-facies anorthosites in which eclogite-facies deformation is mainly localised in crosscutting hydrous eclogite shear zones (e.g. Austrheim and Griffin, 1985; Boundy et al., 1992). Field measurements show a positive correlation between the width W of shear zones and the total displacement D they accommodated (Boundy et al., 1992; Raimbourg et al., 2005). This positive correlation has been observed in others geological contexts (see Fig. 18 of the review paper of Fossen and Cavalcante, 2017), and can either be caused by progressive widening of the shear zones, or can be inherited from the precursor structure they exploited (e.g. Mancktelow and Pennacchioni, 2005; Pennacchioni, 2005). As an example, a set of shear zones from the Neves area (Tauern window, Italy, Pennacchioni and Mancktelow, 2018) show a

tendency towards increasing D with increasing W , but without widening beyond the original extent of the precursor structure. Instead, the shear zone width, length and strain gradients are inherited from the overprinted structure that acted as a nucleation site.

However, in Holsnøy several arguments indicate that the D - W correlation is rather due to the widening of the eclogite shear zones: (1) Between major shear zones (> 100 m wide) and the granulite host-rock, Jolivet et al. (2005) and Zertani et al. (2019) observed a transitional zone, formed by networks of smaller and narrower shear zones delimiting metre-scale granulite blocks. This progressive transition suggests that the small shear zones are an intermediate state of development of larger and wider shear zones, implying that they widen over time. (2) Major eclogite shear zones enclose rotated and scattered metre-scale granulite boudins, within which the orientation of the granulitic foliation varies (Boundy et al., 1992; Jolivet et al., 2005). These boudins are the same size as the blocks delimited by minor shear zones in the outer zone of the major shear zones, and can be considered as their later evolution at larger finite strain. (3) Using a scale-independent numerical model, Kaatz et al. (2021) also showed that Holsnøy shear zones widen over time, owing to synchronous fluid infiltration and deformation. (4) Deformation experiments by Incel et al. (2020) showed that fluid influx and subsequent metamorphic reactions in plagioclase-rich rocks result in the widening of shear zones at eclogite facies conditions.

Such widening can occur if the viscosity contrast between the shear zone and the host rock decreases over time. Viscosity contrast can be reduced either by mechanical weakening of the host rock (e.g. Oliot et al., 2019; Goncalves et al., 2012), or by strengthening of the shear zone itself (e.g. Steffen et al., 2001; Vitale and Mazzoli, 2008). In Holsnøy, the widening of the shear zones is inferred to occur by weakening of the granulite host-rock, due to its eclogitisation promoted by fluid infiltration (e.g. Austrheim, 1987; Kaatz et al., 2021). As eclogite facies deformation was localised within eclogite shear zones, eclogite is considered to be a mechanically weaker rock than granulite (e.g. Austrheim, 1991; Bjørnerud et al., 2002; Jolivet et al., 2005; Raimbourg et al., 2005), and the widening is considered to be only caused by weakening of the host rock (Kaatz et al., 2021). However this does not take into account the kinetics of the metamorphic reactions responsible for eclogitisation, and the potential complex change in strength during the granulite to eclogite transition. As an example, the relationship between deformation and metamorphic reactions has been studied in eclogite facies shear zones in the Sesia Zone (Koons et al., 1987; Rubie, 1998), and in an amphibolite facies shear zone in the Tauern window

(Steffen et al., 2001). In both cases the authors showed that transient weakening can be a prominent process operating during the evolution of the shear zones: rocks weaken during the first stage of metamorphic reaction, and thus localise deformation within a shear zone. During a later stage of reaction, the strength of the rocks is restored. The first weakening stage of the reacting rock can be caused by several mechanisms (Fossen and Cavalcante, 2017):

1. Reaction softening, i.e. the replacement of mechanically strong phases by weaker phases such as mica (e.g. Rubie, 1990; Gueydan et al., 2003; Oliot et al., 2010)
2. Hydrolytic softening, i.e. introduction of water into the crystal lattice of nominally anhydrous minerals, reducing the intercrystalline rock strength and promoting a switch in deformation mechanism (e.g. Tullis and Yund, 1987; Stünitz and Tullis, 2001; Chen et al., 2006; Kohlstedt, 2006).
3. A reduction in grain size (e.g. Rutter and Brodie, 1988b; Handy, 1989; Klaper, 1990).
4. The development of a foliation that increases connectivity between weak phases (Handy, 1990, 1994).

A later "re-hardening" stage of the reacting rock can be caused either by the replacement of weaker phases by stronger ones (Steffen et al., 2001) or by an increase in grain size (Koons et al., 1987).

Additionally, the literature abounds with description of transient weakening processes such as transformation plasticity, dissolution precipitation creep or grain boundary sliding that enhance the deformability of transforming rocks (e.g. Poirier, 1982; Brodie and Rutter, 1985, 1987; Rutter and Brodie, 1988a, 1995; Marti et al., 2018; Stünitz et al., 2020), regardless of the rheological properties of the reaction products. Enhanced deformability is no longer active at the completion of the reaction, the rock behavior being then governed by the properties of the reaction products.

However, transient weakening during the granulite to eclogite transition has yet to be explored in Holsnøy shear zones. In order to constrain the rheological evolution of the granulite during deformation at eclogite facies in Holsnøy, a detailed petrological study of a shear zone extending from the unaltered granulite protolith to the transformed eclogite is required. Matthey et al. (1994) studied the transformation of granulite to eclogite across a metre-scale shear zone in Holsnøy. They however focused on the composition of the fluids infiltrating the shear zones, and did not explore the rheological impact of the metamorphic reactions. In this contribution, we present a detailed petrological study of two eclogite shear zones, extending from the granulite host-rock to the eclogite core. We describe in detail the mineralogical and textural changes

associated with progressive eclogitisation. Based on these and field observations, we argue that the granulite to eclogite transformation induces transient weakening of the reacting rock. We then establish the role of transient weakening using a one-dimensional numerical model of a hydrous, reacting shear zone. We show that the geometry and petrological pattern of metric-scale eclogite shear zones is not controlled by the rheology of eclogite, but rather by the rheology of the transient assemblage. We also investigate values for fluid diffusivity and reaction rates by comparing the numerical results to our field data.

2. Geological setting

Holsnøy Island, in southwestern Norway, belongs to the Lindås nappe (Fig. 1), a part of the Bergen Arcs thrust sheets that formed during the Scandian collisional phase of the Caledonian orogeny (Roberts, 2003). The outcrops studied here are located on northwestern Holsnøy, and are composed of anorthositic granulites that are partially eclogitised. The granulite facies event occurred at 930 Ma during the Grenvillian orogeny (Bengen et al., 2001), during which the rocks equilibrated at temperature (T) and pressure (P) conditions of 800 - 850 °C and < 10 kbar (Austrheim and Griffin, 1985).

The anorthositic granulite was part of the Jotun-Lindås micro-continent, along the hyper-extended margin of Baltica, and was subducted during collision between Baltica and Laurentia (Andersen et al., 1991; Jakob et al., 2017). Bhowany et al. (2018) determined peak P - T conditions for eclogite facies metamorphism in Holsnøy at 670-690 °C, 21-22 kbar. The eclogite facies event has been dated at 435 - 420 Ma (Glodny et al., 2008; Jamtveit et al., 2019). Despite residing at eclogite facies conditions during several Ma (Glodny et al., 2008), the granulite remained partly untransformed. As hydrous minerals (zoisite, phengite) are part of the eclogite paragenesis, and as fluid is a catalyst for metamorphic reactions (Rubie, 1986; Putnis and Austrheim, 2010), the availability of fluid has been inferred as the limiting factor for eclogitisation of the metastable granulite (Austrheim, 1987; Jamtveit et al., 1990).

The widely accepted scenario invoked to explain the formation of Holsnøy eclogite shear zones (Austrheim, 1987; Boundy et al., 1992; Raimbourg et al., 2005; Jamtveit et al., 2018; Zertani et al., 2019; Kaatz et al., 2021) can be summarised as follow: (1) Lower-crustal earthquakes propagated fractures in the brittle granulite. (2) Those fractures acted as a pathway for fluid infiltration into the granulite. (3) The presence of fluids triggered eclogitisation of the granulite

located in undeformed hydration halos surrounding the initial fractures, typically a few tens of centimetres wide. The eclogitisation weakened the granulite located within the hydration halos. (4) Once the eclogitised halos were sufficiently weakened, they started to deform in a ductile manner, so that they were the precursor structures of small-scale eclogite shear zones that localised deformation. (5) The shear zones widened owing to diffusion of the fluid along a pressure gradient orthogonal to the shear direction. (6) Multiple shear zones coalesced into shear zone networks, then into major 100-m wide eclogite shear zones that enclose preserved granulite blocks.

Large areas of Holsnøy also show a partial "static" eclogite facies overprint of the granulite, which was associated with fluid infiltration but no deformation (Zertani et al., 2019).

3. Analytical methods

Two 1 metre-wide shear zones, located on Figure 1, were sampled from their margin to their core. Photographs and interpretative sketches of the shear zones along with sample locations are shown in Figure 2. Since the outcrops are horizontal with almost no topography, eclogite lineations could not be measured accurately. However regional lineation measurements by Boundy et al. (1992), Raimbourg et al. (2005) and Kaatz et al. (2021) show that shear zones regionally have a lineation dip between 10 and 30° toward the East. The outcrop surface is therefore close to the shear zone XZ plane, with X parallel to the movement direction and Z orthogonal to the shear plane.

Thin sections were analysed with scanning electron microscopy (SEM) to obtain 2.25 x 1.69 mm EDS (Energy-dispersive spectroscopy) chemical element maps of representative areas (e.g. coronas, matrix). Quantitative mineral compositions were measured using electron probe micro-analysis (EPMA). Analyses were performed at IStEP (Sorbonne Université, Paris) using a ZEISS Supra 55 VP Scanning Electron Microscope (spatial resolution 2.2 µm), and at the CAMPARIS facility (Sorbonne Université, Paris) using a CAMECA SX-100 Electron Microprobe (spatial resolution 2 µm).

Grain sizes were quantitatively estimated from EDS maps and photomicrographs using a watershed segmentation algorithm written in MATLAB. EDS maps were processed with MATLAB to compute mineral phase maps (presented in supplementary material A), using a nearest neighbour algorithm: for each map, control points of known mineralogy were identified, using EPMA analyses. The euclidean distance of each pixel to each of the control points was

calculated in a n -dimensional space, where n is the number of chemical elements mapped with EDS. Each pixel was then assigned the mineralogy of the nearest control point. If the distance between a pixel and the closest control point was greater than a preset threshold, the pixel was not indexed. Mineral proportions were then calculated by pixel counting on the phases maps. The proportions of the investigated areas (e.g. coronas, matrix) were estimated in thin sections and hand samples, allowing to calculate the mineral proportions at the sample scale. Compared to other quantitative techniques such as X-ray powder diffraction (XRPD), using EDS maps to quantify the minerals proportions allows to remove the effects of amphibolitisation on the proportions of the eclogite facies minerals. Additionally, as the rocks have a large scale chemical heterogeneity, large volumes of rock would be needed to calculate representative compositions with XRPD. But since we study local equilibria, these volumes may not be representative of the studied domains.

Hereafter, we use the following mineral abbreviations from Kretz (1983): Ab = albite; Alm = almandine; An = anorthite; Cpx = clinopyroxene; di = diopside; grs = grossular; grt = garnet; hd = hedenbergite; jd = jadeite; kfs = K-feldspar; Ky = kyanite; Omp = omphacite; Pl = plagioclase; Prp = pyrope; Qtz = quartz; Zo = zoisite. We also use Amp for amphibole, Ca-ts for Ca-tschermakite and Ph for phengite.

4. Results

4.1. Petrological description

All samples exhibit weak amphibolite-facies retrogression, as shown by amphibole/clinopyroxene - plagioclase symplectites around garnet and omphacite. As retrograde minerals are not the focus of this work, the following section only deals with minerals formed during prograde to peak eclogite metamorphism.

Mineralogical assemblages vary from the margins to the core of the shear zones, and the pattern is similar for both shear zones. From the granulite host-rock to the core of an eclogite shear zone, we identified five petrologically distinct domains:

Domain D0 corresponds to the granulite protolith unaffected by eclogite facies deformation and fluid infiltration. D0 is located at least 0.5 m away from the outer edge of the shear zone (Mattey et al., 1994), and was sampled in SZ1. The unaltered granulite is composed of millimetre-sized grains of plagioclase, garnet, clinopyroxene and minor orthopyroxene and amphibole (Fig. 3d-f). Elongated elliptical pyroxene clusters surrounded by garnets form coronitic

structures that mark the granulite foliation and lineation. Coronas account for around 30 % of the granulite volume, the rest being composed of a matrix of plagioclase and isolated garnets between the plagioclase grains.

Domain D1 is located within 0.5 m of the margin of the shear zone and was sampled in SZ2 (Fig. 2, samples m18a and m18e). The texture is similar to that of D0, with coronas embedded in a matrix that contains isolated garnets (Fig. 3d and e). Although the coarse plagioclase grains of D0 are pseudomorphed in D1 by a new matrix of fine-grained ($< 50 \mu\text{m}$) Ab+Zo+Ky+Ph+Qtz (Fig. 3f), the grain boundaries of former plagioclase grains can still be identified in this new matrix (Fig. 3d).

Clinopyroxenes in the coronas show exsolution lamellae of garnet and rutile (Fig. 3e). Reaction rims around garnets (Fig. 3e and 3f) are composed of a very fine-grained Omp+Zo+Ab+Ky+Ph aggregate. Similar reaction rims are found at the matrix/corona interface.

Domain D2 is located at the edge of the shear zone and was sampled in SZ1. The coronas/matrix structure resembles that of D1, but shows a manifest eclogite facies foliation imprint. Reaction rims around garnet grains and around coronas are wider (Fig. 3g and 3h), and the structure of former D0 plagioclase grains is no longer visible. The composition of the matrix is similar to that of D1, but grains are coarser, up to $100 \mu\text{m}$ (Fig. 3f). Omphacite replaced clinopyroxene in the coronas, which are now mostly composed of Omp+Grt+Ph.

Domain D3 was sampled in both SZ1 and SZ2 (Fig. 2, samples m18b and m18d in SZ2). The coronas/matrix structure is less distinct than in D1 and D2, and the foliation marked by Zo+Ky+Ph+Qtz layers and Omp+Ky layers is clearly defined (Fig. 3j). The Omp+Ky layers mostly develop around coronas and isolated garnets in the matrix (Fig. 3k and 3l). The grain size in the matrix is less than $100 \mu\text{m}$.

Domain D4 is located at the core of the shear zone, and was sampled in both SZ1 and SZ2 (sample m18c in SZ2). The entire domain is very homogeneous, with no coronas/matrix structure and a poorly defined foliation (Fig. 3m and 3n). The mineral assemblage is a typical Omp+Ky+Zo+Grt+Ph \pm Qtz eclogite, with most of the grains coarser than $200 \mu\text{m}$ (Fig. 3o).

4.2. Mineral compositions

The compositions of the minerals are different in SZ1 and SZ2, and are therefore reported separately in Table 1 and Table 2, respectively. Within each shear zone, the composition of

plagioclase, phengite and zoisite only show some minor variations between D2, D3 and D4, and was averaged over these 3 domains (Tables 1 and 2).

The composition of phengite and plagioclase in D1 is different from that of D2, D3 and D4. In particular, the proportion of the anorthite end-member X_{An} in plagioclase is higher in D1 (Table 2: $X_{An} = 0.15$ in D1, $X_{An} = 0.12$ in D3/D4).

All garnets from D1 to D4 show compositional zoning (see an example in supplementary material B), with a core enriched in pyrope end-member X_{Prp} and a rim enriched in almandine end-member X_{Alm} . For example in SZ1 (Table 1), $X_{Alm} = 0.27$ and $X_{Prp} = 0.53$ in the core; and $X_{Alm} = 0.43$ and $X_{Prp} = 0.33$ in the rim. Although the width of the Fe-rich rims increases from D1 to D4, the compositions of cores and rims are similar within each shear zone and were averaged across all domains in tables 1 and 2.

The composition of omphacite varies (1) across the shear zones, between the petrological domains D2, D3 and D4, and (2) between the cores and the matrix of a given domain. In particular, in both shear zones the jadeite end-member proportion X_{jd} in matrix omphacites decreases from the edge (D2) to the core (D4); in SZ1 matrix the jadeite end-member decreases from D2 ($X_{jd} = 0.54$) to D4 ($X_{jd} = 0.50$); and in SZ2 matrix the jadeite end-member decreases from D3 ($X_{jd} = 0.58$) to D4 ($X_{jd} = 0.52$).

4.3. Mineral proportions

Mineral proportions in D0, D1, D2, D3 and D4 were estimated following the method presented in section 3. As they were calculated using small scale EDS maps, the mineral proportions shown in Figure 4 are semi-quantitative. However, they have been chosen to be as representative as possible of the whole studied domain and estimations have been performed on several EDS maps giving comparable results. Although mineral proportions in SZ1 and SZ2 are different, a similar trend is observed: the proportion of omphacite and kyanite increases from D1 to D4 whereas the proportion of zoisite, garnet and plagioclase decreases from D1 to D4.

5. Synthesis on shear zone evolution in Holsnøy

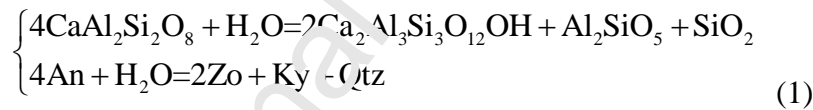
5.1. Succession of metamorphic reactions

Based on our textural and compositional analysis, it is manifest that the eclogite facies imprint increases from the unaltered granulite outside the shear zone (D0) to the eclogite core (D4). We can describe the eclogitisation process across a shear zone as the sequence of mineral reactions (1) to (5), all occurring at around 700 °C, 21 kbar (Bhowany et al., 2018).

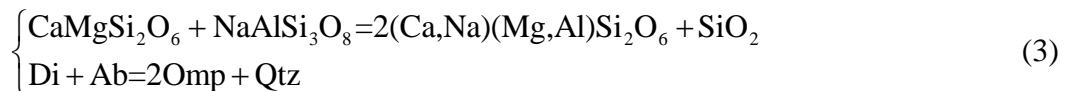
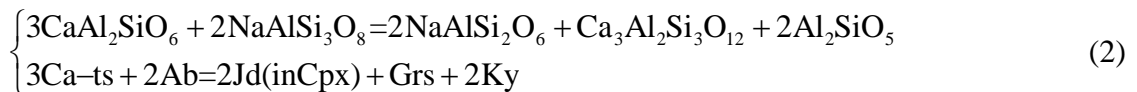
We calculated the bulk composition of each domain using EPMA mineral compositions (Tables 1 and 2), mineral proportions (Fig. 4) and mineral densities at eclogite facies conditions (700 °C and 2GPa) from the Abers and Hacker (2016) database. The results, presented in supplementary material C, suggest that, other than the introduction of volatile elements, the formation of metric-scale eclogite shear zones can be considered as essentially isochemical. We therefore balance the reactions considering H₂O as the only mobile species.

The reactions are presented in chronological order, from stages D0 to D4. Relative solid volume change and total volume change have been computed for each of the reactions, based on the Abers and Hacker (2016) database, with 1100 kg/m³ used for the water density (Brodholt and Wood, 1993).

From D0 to D1. In the matrix, the anorthitic component of the granulitic plagioclase (An₄₀) reacts to form zoisite, due to the hydration of the granulite:



This reaction has been described by numerous authors (e.g. Jamtveit et al., 1990; Matthey et al., 1994). The change in solid volume associated with this reaction is -14 %, and the change in total volume is -18 %. This reaction leaves the albitic component of plagioclase untransformed, forming the Ab+Zo+Ky+Ph+Qtz matrix of D1. Phengite was not included in the reactions but is also a product of plagioclase destabilisation (K-feldspar end-member). Albite only reacts at the coronas/matrix interface to form omphacite, following the reactions:

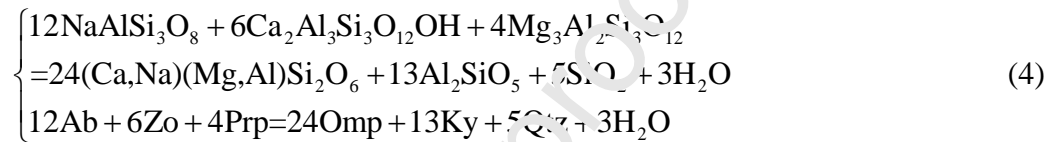


A reaction similar to reaction (2) has been described by Raimbourg (2005), and a reaction similar to reaction (3) has been described by Matthey et al. (1994) and Schneider et al. (2007). The changes

in volume associated with reactions (2) and (3) are respectively -13 % and -10 %. The exsolution lamellae of garnet in clinopyroxene observed on Figure 3e are interpreted as the product of reaction (2).

From D1 to D2. Reaction (1) leaves the remaining plagioclase with an average Ab_{86} composition in D2 (Table 1). As in D2, D3 and D4 the composition of plagioclase is the same (average Ab_{86}), reaction (1) is considered as complete in D2. Reaction (3) continues until all the former millimetric grains of clinopyroxene react to form small omphacite grains.

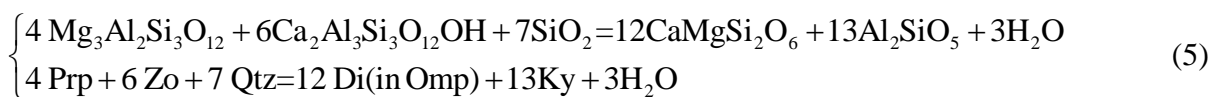
The albitic plagioclase and zoisite in the matrix react with garnets (isolated grains or in the coronas) following the reaction:



Similar reactions have been described by Matthey et al. (1994) and Schneider et al. (2007). The change in solid volume associated with this reaction is -10 %, and the change in total volume is -8 %. The contribution of garnet to the reaction is manifest from the reaction rims around isolated garnets and coronas (Fig. 3g to 3l). The zoning of garnet is also consistent with this reaction: as pyrope preferentially contributes to reaction (4), the garnet rims are enriched in almandine (see supplementary material B). Reaction (4) can be observed in Figure 3h, where the mineral composition of the corona (omp+grt) is noticeably different from the composition of the corona/matrix interface (omp+iv). The omp + ky assemblage is the product of reaction (4). Reactions (2), (3), (4) are balanced without including the minor remaining anorthitic component of plagioclase, although it is also consumed by the reactions as a Ca-bearing reactant.

From D2 to D3: Reaction (4) proceeds until all the plagioclase is consumed. The product of this reaction is evidenced in Figures 3h and 3i, where a rim of Omp+Ky separates the garnets from a matrix composed mostly of Zo+Ky \pm Qtz and very little plagioclase.

From D3 to D4: The proportion of omphacite and kyanite increases, at the expense of zoisite and quartz. Additionally the jadeite content of omphacite in the matrix decreases. This can be explained by the following reaction taking place in the matrix:



The change in solid volume associated with this reaction is -4 %, and the change in total

volume is -1 %. Compared to the earliest reactions in the sequence, reaction (5) causes the smallest decrease in volume.

5.2. *Shear zones evolution and rheological implications*

As Holsnøy shear zones widen over time (e.g. Jolivet et al., 2005; Kaatz et al., 2021), the spatial evolution from D0 to D4 described by the sequence of reactions (1) to (5) can be interpreted as a proxy for the temporal evolution of the granulite, from unreacted to fully eclogitised. We use this interpretation as a working hypothesis in the following section. Using this hypothesis, a schematic diagram illustrating the spatial and temporal evolution of a metre-scale shear zone is presented in Figure 5. The transformation of granulite into eclogite can be subdivided into two successive stages, occurring at the same eclogite facies conditions, that both have a prominent effect on the strength of the transforming rock:

(i) Destabilisation of the metastable granulite assemblage (D0) into a transient assemblage (D3), following reactions (1) to (4). They can syntactically be combined as:



During this first stage, the grain size decreases, weak phases (phengite, quartz) replace strong phases (plagioclase, garnet), fluid content increases and solid volume strongly decreases. These changes have a pronounced weakening effect on the rock (e.g. Poirier, 1982; Klaper, 1990; Jamtveit et al., 2019).

(ii) Destabilisation of the transient assemblage (D3) into eclogite (D4), following reaction (5). During this second stage, the grain size increases, the fluid content decreases and the solid rock volume shrinking is minor (-4 % to be compared to -14 % for reaction 1). These changes have an overall strengthening effect on the rock. This suggests that fully-reacted eclogite in the core of the shear zone (D4) is stronger than the rock still undergoing reaction (6) on the edge of the shear zone.

The strength contrast within a shear zone can also be distinguished at the outcrop scale. This is best seen on Figure 2b, where the eclogite facies foliation at the edge of the shear zone (D2-D3) is more pronounced than in the central part (D4). This suggests that instantaneous shear is higher at the edge than in the core, and therefore that the edge is weaker than the core. It is inferred that the completion of the reactions sequence hardened the core of the shear zones with growth of strong and coarser minerals, moving the deformation towards the peripheral, transiently

transformed domains that contain weaker phases. The preservation of the granulite-facies coronas in the shear zone edges and their dismantling in the core of the shear zones also implies a decreasing strength contrast between the coronas and the matrix toward the shear zone cores.

These observations show that eclogitisation does not simply gradually weaken the rock from the granulite initial strength down to the eclogite end-product strength, but rather constitutes a two-stage evolution. First, the granulite (D0) transforms into a "reacting granulite" (D3), weaker than the granulite and the final eclogite, that localises the deformation. Second, the reacting granulite transforms into final eclogite (D4). This second stage partially restores the strength of the rock to reach the final steady-state strength of the eclogite. In order to test this hypothesis, we built a one-dimensional numerical model that aims at reproducing the geometry and petrology of the shear zones from Holsnøy. We also use this model to constrain the fluid diffusivity and the metamorphic reaction rate in the shear zone.

6. One dimension numerical model of an eclogite shear zone

6.1. Model description and equations

The time evolution of a hydrous reacting shear zone was modelled in one dimension (1D) using MATLAB. As boundary conditions and geometry are symmetric, only the half-width of a shear zone, from core to edge, was modelled.

The initial setup is summarised in Figure 6a. Initially the entire 1D space consists of metastable granulite, which does not transform into eclogite because of the lack of fluid. At the onset of deformation, simple shear is applied on the model by imposing a horizontal velocity at the top. Simultaneously, a finite amount of fluid is injected at the lower boundary, simulating a pulse of fluid through a fracture.

Fluid propagation in the granulite is modelled with a diffusion equation, as in Kaatz et al. (2021). As the fluid propagates outwards, the eclogitisation reaction starts in the granulite. The evolution of the rock strength reproduces the two-stages rheological evolution deduced from our petrological observations (Fig. 6b). First, the granulite transforms into a reacting granulite which is weaker than the initial granulite. Second, the reacting granulite transforms into eclogite, which is stronger than the reacting granulite.

The fluid is not only a catalyst for the metamorphic reaction, but also a reactant and product of the metamorphic reactions occurring in a shear zone (see reactions in section 5.1, and Fig. 5).

Therefore, as the reaction progresses, the rock consumes or releases free fluid available for diffusion in the shear zone (Fig. 6b). The final state of one simulation is shown on Figure 7.

For simplification, only viscous deformation is accounted for in this model, and volume changes associated with the reactions are not considered. The equations are discretised over the 1D space using finite differences. The values of the parameters are described in section 6.2 and Table 3.

The propagation of free fluid F is modelled with a diffusion equation:

$$\frac{\partial F}{\partial t} = D \frac{\partial^2 F}{\partial y^2}, \quad (7)$$

where D is the constant of fluid diffusivity, t is the time and y is the 1D spatial coordinate.

As fluid acts as a catalyst, the eclogitisation reaction is modelled with a linear law involving the constant of reaction rate α_r and the amount of free fluid F :

$$\begin{cases} \frac{\partial r}{\partial t} = \alpha_r \times F & \text{if } F < 1, \\ \frac{\partial r}{\partial t} = \alpha & \text{if } F > 1, \end{cases} \quad (8)$$

where r is the progress of the granulite to eclogite reaction: $r = 0$ corresponds to unaltered granulite, and $r = 1$ to fully reacted eclogite. When $F < 1$, the amount of fluid controls the rate of eclogitisation. When $F > 1$, fluid saturation is reached, i.e. adding more fluid does not increase the reaction rate.

As the reaction progresses, the reacting rock consumes or releases free fluid (Fig. 6b). The exchange of fluid is modelled with a 2-steps linear law:

$$\begin{cases} \frac{\partial F}{\partial r} = \frac{f_r - f_g}{r_t} & \text{if } r < r_t, \\ \frac{\partial F}{\partial r} = \frac{f_e - f_r}{r_t} & \text{if } r > r_t, \end{cases} \quad (9)$$

where f_g , f_r and f_e are the amounts of constitutive fluid in the granulite, reacting granulite and eclogite, respectively. r_t is the threshold at which the reaction switches from a weakening behaviour to a strengthening behaviour. $r < r_t$ corresponds to the weakening stage of the reaction, and $r > r_t$ to the strengthening stage. The solutions of equations involving fluid (equations 7, 8, 9)

are solved through convergence of Picard iterations.

The rheology of end-member lithologies (10) is computed using a viscous rheological model following the dislocation creep equation (11):

$$\sigma = 2\eta\dot{\epsilon}, \quad (10)$$

$$\eta = \frac{\dot{\epsilon}^{\frac{1-n}{n}}}{2 \left[A \times \exp\left(\frac{-Q}{RT}\right) \right]^{1/n}}, \quad (11)$$

where σ is the stress, $\dot{\epsilon}$ the strain rate, A the pre-exponential factor, n the stress exponent, Q the activation energy, T the temperature, and R the universal gas constant. A , n and Q are dislocation creep constants of a given end-member lithology (granulite, reacting granulite or eclogite).

The strength of the reacting rock is calculated from the strength of end-member lithologies using the minimised power geometric (MPG) model of Huet et al. (2014) (Fig. 6b). Calculations of intermediate strengths using the Reuss lower bound (weighted harmonic mean of the end-member viscosities, Reuss, 1929) or the Voigt upper bound (weighted arithmetic mean, Voigt, 1928) do not yield widely different results and lead to the same conclusions than the MPG model (see supplementary material D).

The Stokes equation, simplified for 1D simple shear with no inertial forces, is solved to calculate the velocity in the x direction V_x :

$$\frac{\partial(\eta \times \frac{\partial V_x}{\partial y})}{\partial y} = 0. \quad (12)$$

As the viscosity is nonlinear ($n \neq 1$ in equation 11), equation 12 is solved through convergence of Picard iterations.

6.2. Model parameters

This section details how the parameters used in the model are determined. Their values are summarised in Table 3.

Background strain rate ($\dot{\epsilon}$). We use a strain rate of $\dot{\epsilon} = 10^{-14} \text{ s}^{-1}$, consistent with the estimate of $\dot{\epsilon} = 10^{-14 \pm 1} \text{ s}^{-1}$ by Fagereng and Biggs (2019) for crustal strain rate.

Duration of the model (t). The half-width (from core to border) of both SZ1 and SZ2 is about 0.6m. It was impossible to measure the offset of the shear zones on the field, however Boundy et al. (1992); Kaatz et al. (2021) reported that the offset of minor shear zones (< 1m wide) is approximately equal to their width. The offset of SZ1 and SZ2 is therefore considered to be around 0.6m.

In this model, the shear zone offset d depends only on the strain rate and on the model duration:

$$d = 2\dot{\epsilon}Lt, \quad (13)$$

where L is the length of the model. Using $L = 2\text{m}$, an offset of 0.6m and a strain rate of 10^{-14} s^{-1} , this yields $t \approx 0.5\text{Ma}$.

Fluid concentration in rock (f_g, f_r, f_e). Using the proportions of hydrated phases (zoisite, phengite) given in Figure 4, we calculated that the mass fraction of fluid is around $f_g = 0$ wt % in the granulite, $f_r = 0.5$ wt % in the reacting granulite and $f_e = 0.25$ wt % in the eclogite. As the mass fraction is dimensionless and the model is one-dimensional, the unit of fluid concentration is cm^{-1} .

Amount of fluid in initial pulse (F_0). This parameter is poorly constrained. However, the total amount of fluid must be somewhat limited, otherwise it would propagate after the deformation is achieved. For this reason we set the initial amount of fluid to be equal to the maximum theoretical amount of fluid contained in the rock: $F_0 = f_r \times L = 0.5 \times 200 = 100$. This amount is dimensionless.

Temperature (T). We used a constant temperature of $T = 700\text{ °C}$, close to that determined by Bhowany et al. (2018) for the peak eclogite facies metamorphism in Holsnøy (670-690 °C).

End-member rheology (n, A, Q, η). We used experimentally determined rheologies to model the rheology of granulite, reacting granulite and eclogite. We used the creep parameters of dry anorthite determined by Rybacki and Dresen (2000) to model the rheology of granulite, and creep parameters of omphacite determined by Zhang et al. (2006) to model the rheology of eclogite. Our previous observations suggest that the reacting granulite is the weakest phase. For this reason it was modelled by quartz, which is weaker than both anorthite and omphacite. We used

the creep parameters of quartz determined by Hirth et al. (2001). At $T = 700$ °C and $\dot{\epsilon} = 10^{-14}$ s⁻¹, the strength ratios are $\eta_t/\eta_g \approx 1/38$ and $\eta_e/\eta_g \approx 1/23$, which compares to previous estimates for the same contexts (Labrousse et al., 2010).

Reaction threshold (r_t). Tests performed using different r_t values show that model results are not widely different if r_t varies from 0.1 to 0.9 (see supplementary material E). As the kinetics of reaction is poorly constrained we chose a median value of $r_t = 0.5$.

6.3. Role of diffusivity and reaction rate

In a first parametric study we determine realistic values of fluid diffusivity D and metamorphic reaction rate α_r , using the end-member rheologies chosen in section 6.2. In order to assess the validity of a model, we compare the petrology and geometry of the modelled shear zones to those observed on the field. Key constraints are:

1. the half width of the shear zone, $W \approx 0.6$ m on the field (Fig. 2). As the width of a single shear zone can significantly vary on the field, we consider that the width of a modelled shear zone must be $W = 0.6 \pm 0.4$ m.
2. the petrology of the shear zone. The core of the shear zone is eclogite (D4) while the edge is reacting granulite (D2-D3). We implement this constraint in the model by monitoring the width of the eclogite core (W_e), relative to the width of the entire shear zone (W). As both the eclogite and the reacting granulite must coexist in the shear zone, we consider that W_e/W must be between 0.1 (10 % of the shear zone is fully reacted eclogite) and 0.9.
3. the petrology outside the shear zone. On the field, D1 is within 0.5 m of the edge of the shear zone and has already started the metamorphic reaction, therefore the host-rock within a few tens of centimetres of the modelled shear zone must be reacting granulite.

On the figures, granulite is defined by $r < 0.05$, reacting granulite by $0.05 \leq r < 1$, and eclogite by $r = 1$.

There is a trade-off between the duration, t , and values of D , α_r and $\dot{\epsilon}$. For instance the model yields the same results if t is multiplied by 10, and D , α_r and $\dot{\epsilon}$ are all divided by 10. For this reason we can normalise D and α_r to $\dot{\epsilon}$. This allows us to study the role of

diffusivity and reaction rate independently of $\dot{\epsilon}$. In order to investigate the role of D and α_r , we ran the model for a range of diffusivity values between $10^{-3} \times \dot{\epsilon}$ and $10^3 \times \dot{\epsilon}$, and a range of reaction rate values between $10^{-1} \times \dot{\epsilon}$ and $10^4 \times \dot{\epsilon}$. The results of this parametric study are shown in Figure 8.

Different $D-\alpha_r$ combinations produce shear zones with widely varying geometry and petrology. A slow diffusivity and a fast reaction rate produce a shear zone where all the fluid remains in a narrow zone which reacts quickly. The final shear zone is very narrow, and has fully reacted (Fig 8, model 1). A fast diffusivity and a slow reaction rate produce a zone that widens rapidly and consumes all the fluid in the reacting granulite, such that there is no more fluid left to catalyse the reaction. The shear zone is therefore wide but its core has not transformed into eclogite (Fig. 8, model 3). A very slow reaction rate and/or a very fast diffusivity do not result in the formation of a shear zone because the granulite is not weakened enough to localise deformation (Fig. 8, model 4). Only a small range of D and α_r values ($D/\dot{\epsilon} = 10^{-2} - 10^1$, $\alpha_r/\dot{\epsilon} = 10^1 - 10^2$) results in shear zone geometry and petrology similar to those observed in the field (Fig. 8, model 2): (1) the width is $\approx 0.6\text{m}$; (2) the shear zone consists of an eclogite core and a reacting edge; and (3) the granulite started to react within 50 cm of the edge of the shear zone.

6.4. Role of viscosity changes

The strength of the different end-member lithologies, and especially of reacting granulite, is not well constrained. For this reason we conducted a second parametric study in order to constrain the relative strengths of granulite, reacting granulite and eclogite. We used the parameters in Table 3 and realistic values of D and α_r determined in section 6.3: $D/\dot{\epsilon} = 1$, $\alpha_r/\dot{\epsilon} = 10$. We set the strength of granulite to $\eta_g = 1$, and tested a range of reacting granulite strength (η_t) and of eclogite strength (η_e), relative to that of granulite. The results of this parametric study are shown in Figure 9.

For $\eta_t > \eta_e$ ("transient strengthening", Fig. 9, model 5), the shear zone is entirely composed of eclogite. Reacting granulite is only present outside the shear zone, but not on the edge of the shear zone. This model does not reproduce the observed petrology, which shows that the transient rheology can not be stronger than the end-product eclogite.

For $\eta_t < \eta_e$ and $\eta_t < \eta_g$ (Transient weakening, Fig. 9, models 6 and 7), the geometry and petrology of the shear zones are realistic and similar to that of model 2 (Fig. 8). The models are realistic even if the final eclogite is stronger than granulite (model 7), as long as transient weakening occurs during the reaction.

Our numerical simulations reproduce realistic shear zones patterns only in a narrow parametric space: $D/\dot{\epsilon} = 10^{-2} - 10^1$, $\alpha_r/\dot{\epsilon} = 10^1 - 10^2$, $\eta_t/\eta_g < 1$, $\eta_t/\eta_e < 1$. Out of this $D-\alpha_r-\eta_t-\eta_e$ space, modelled shear zones are too localised or too diffuse, or their petrological pattern does not match that observed on the field.

7. Discussion

7.1. Chemical equilibrium

An important field observation is that the granulite is chemically heterogeneous at the cm-, and even dm-scale, as inferred from the coronas/matrix texture. We have shown that this heterogeneity is well preserved in the shear zone and only disappears in the core of the shear zone (D4), where the metamorphic reactions sequence (1) to (5) is complete. Similarly, there is a compositional heterogeneity of omphacite in the shear zone that only disappears in the core (Tables 1 and 2). In particular, in D2 and D3 the omphacites of the coronas and the omphacites of the matrix have a different composition. For example in D2, $X_{jd} = 0.42$ in the coronas and $X_{jd} = 0.54$ in the matrix (Table 1). In D4 the composition of omphacite is the same in the coronas and in matrix. These changes in omphacite composition can be caused by changes in the equilibrium bulk composition, but we showed that minor shear zones in Holsnøy are essentially isochemical. It is therefore likely that the composition of omphacite is controlled by local chemical equilibrium in distinct petrological domains of varying scale, at constant eclogite facies $P-T$ conditions. In D2 and D3, the omphacites are in equilibrium with different local chemical compositions (matrix vs corona). Likewise, the transient eclogite assemblage in D1-D3 is a result of a local chemical equilibrium. Metamorphic reactions, deformation and fluid assisted chemical diffusion progressively equilibrated the reacting rock at larger scale, until the eclogite became texturally and chemically homogeneous in the core of the shear zone. If the transformation of granulite into eclogite happened instantaneously, with a large scale (over tens of centimetres)

equilibrium composition, then the entire shear zone would always be composed of "true" eclogite as observed in the core: $\text{Omp} + \text{Ky} + \text{Grt} + \text{Zo} + \text{Ph} + \text{Qtz}$. However, because of spatial disequilibrium and reactions kinetics, the margin of the shear zones, which started reacting the latest, consist of a transient transforming assemblage. Observations of such equilibration in shear zones were also made by Koons et al. (1987) in the Sesia zone (Alps), by Mørk (1985) in Flemsøy (Western Norway), or by Goncalves et al. (2012) in the Aar massif (Alps).

7.2. *Causes of transient weakening*

In this work we showed that transient weakening must have occurred in the Holsnøy shear zones, but the mechanisms causing the change in rheology are poorly understood. Dislocation creep probably dominates the deformation mechanisms in omphacite (Boundy et al., 1992; Godard and van Roermund, 1995; Bascou et al., 2001, 2002) and kyanite (Beane and Field, 2007); however transient mechanisms activated during a metamorphic reaction can enhance deformation of the transforming rock (Brodie and Rutter, 1985; Rubie, 1990; Rutter and Brodie, 1995). We therefore propose the following interpretation for the evolution of rheology during the eclogitisation of granulite:

(1) During the first stage of eclogitisation (D0 to D3, i.e. reactions 1 to 4), most of the original coarse (>1 mm in diameter) granulite facies minerals (plagioclase, pyroxene) are replaced by small eclogite facies minerals (omphacite, zoisite, kyanite), as illustrated on figures 4 and 5. The intense mineral replacement, grain size reduction and volume reduction are inferred to activate transient deformation mechanisms that weaken the transforming rock: diffusion creep during dissolution of granulite minerals and precipitation of eclogite minerals (e.g. Stünitz and Tullis, 2001; Marti et al., 2018; Stünitz et al., 2020), grain boundary migration in dynamically recrystallised small plagioclase grains (Klaper, 1990), transformation plasticity during volume reduction (Poirier, 1982). The volume reduction also yields an increased porosity which can weaken the solid framework and change the fluid pressure field, promote fluid influx and further promote the reaction (Kaatz et al., 2021). The fine-grained matrix forms interconnected weak layers that accommodate most of the strain (Klaper, 1990; Handy, 1990, 1994).

(2) Contrary to the first stage, the second stage of eclogitisation is not marked by intense mineral replacement but rather by a textural and chemical equilibration induced by reaction (5) (compare D3 and D4 panels on figure 5). We therefore expect the weakening induced by the

previous transient processes to be limited during this reaction stage. On the contrary, the textural and chemical equilibration increases the grain size and obliterates the interconnected weak layers structure, which hardens the reacted eclogite.

It is out of the scope of this study to determine the deformation mechanisms at work in the shear zones, and for this reason the rheology of the rocks is only modelled by dislocation creep in our numerical model. Taking into account transient deformation mechanisms as described above, such as diffusion creep during the metamorphic reaction (e.g. Stünitz et al., 2020), would amplify the importance of transient weakening on the evolution of the shear zones.

In the shear zones studied in this work, only the core of the shear zone, which started the reaction the earliest and underwent more strain and fluid infiltration, could complete the hardening stage of eclogitisation. The edge, which started the reaction later, only underwent the weakening stage of eclogitisation.

7.3. *End-members rheologies*

The numerical models show that the transient weakening of the granulite undergoing the metamorphic reaction is necessary to explain the geometry and petrology of the shear zones observed in the field. However our model does not constrain the relative strengths of granulite and eclogite: as long as the transforming rock goes through a weak transient stage, the model yields realistic results, regardless of the rheology of the protolith and of the final transformed assemblage.

7.4. *Role of eclogite hardening on shear zones widening*

The acknowledged interpretation of the evolution of Holsnøy shear zones is that only fluid infiltration is responsible for shear zone widening (e.g. Austrheim, 1987; Kaatz et al., 2021). Figure 10 shows a comparison between this classical scenario (case A) and transient weakening associated with a fluid infiltration scenario (case B). Both cases use the same parameters, although the evolution of rock strength is different (Fig. 10a). In case A the rock strength gradually decreases from granulite strength at $r=0$ to eclogite strength at $r=1$. In case B the strength evolution follows the two stages described in the previous models. In case A the shear zone is 44 cm wide while in case B it is 62 cm wide. This substantial width increase (+18 cm, i.e. +40 %) is due to the hardening stage: progression of the reaction in the core pushes strain localisation

outwards from the shear zone (Fig. 10c) and hence promotes shear zone widening. The strain partition in the shear zone is similar to that of paired shear zones (Mancktelow and Pennacchioni, 2005), with a hardened central part and the margins undergoing most of the strain. However, our model shows that since the shear zones are continuously expanding and transforming due to fluid infiltration, they do not evolve into paired shear zones but rather into shear zones with a sigmoid-shape foliation, as observed on the field. No change in reaction kinetics induced by strain or strain rate has been accounted for in our model, but such feedback mechanisms would amplify the process presented here (e.g. Snow and Yund, 1987; Yund and Tullis, 1991). Therefore, although shear zone widening is mostly controlled by fluid diffusion that weakens the rock, the hardening of the eclogite at the end of the metamorphic reaction also plays an important role in the widening of the shear zone.

7.5. *Fluid supply in the shear zones*

The fluid supply can be modelled by a continuous influx or an instantaneous pulse of fluid (Kaatz et al, 2021). In Holsnøy, fluid infiltration was induced by earthquakes in brittle granulite. This argues in favour of infiltration by instantaneous fluid pulses following earthquakes (as in Malvoisin et al., 2020) and for this reason we used this hypothesis in the model.

For the sake of completeness, we tested a scenario where the fluid continuously infiltrates the granulite, as in the model of Kaatz et al. (2021). Assuming that the total amount of fluid injected into the shear zone is the same in both scenarios, we used a continuous influx of fluid of $Q = F_0 / t = 6.4 \times 10^{-12} \text{ s}^{-1}$. The results of this model (shown in supplementary material F) show similar results to our scenario that uses pulsed fluid. The only difference is that the continuous influx model allows for lower fluid diffusivity, in agreement with the value determined by Kaatz et al. (2021). Therefore, although the regime of fluid infiltration in Holsnøy is poorly understood, it has little implications on the conclusions presented here.

7.6. *Fluid diffusivity and reaction rate*

Constraining the parametric study with field observations, we found $D / \dot{\epsilon} = 10^{-2} - 10^1$ and $\alpha_r / \dot{\epsilon} = 10^1 - 10^2$ as realistic diffusivity and reaction rate values, respectively (Fig. 8). With a strain rate of $\dot{\epsilon} = 10^{-14} \text{ s}^{-1}$ used in the model, this yields $D = 10^{-16} - 10^{-13} \text{ m}^2 \cdot \text{s}^{-1}$, and

$\alpha_r = 10^{-13} - 10^{-12} \text{ s}^{-1}$. Another commonly used value of strain rate in Holsnøy is $\dot{\epsilon} = 10^{-13} \text{ s}^{-1}$ (Labrousse et al., 2010; Kaatz et al., 2021). Using this value yields $D = 10^{-15} - 10^{-12} \text{ m}^2 \cdot \text{s}^{-1}$, and $\alpha_r = 10^{-12} - 10^{-11} \text{ s}^{-1}$. We therefore consider that reasonable values for Holsnøy shear zones are $D = 10^{-14 \pm 2} \text{ m}^2 \cdot \text{s}^{-1}$ and $\alpha_r = 10^{-12 \pm 1} \text{ s}^{-1}$.

Our reaction rate is higher than those compiled by Baxter (2003) in natural rocks undergoing regional metamorphism ($6 \times 10^{-16} - 6 \times 10^{-14} \text{ s}^{-1}$). It is close to the upper bound of reaction rate determined by Cruz-Urbe et al. (2014) in mafic rocks, using Nb diffusion in rutile and titanite ($4 \times 10^{-16} - 2 \times 10^{-13} \text{ s}^{-1}$). The difference in reaction rate magnitudes is likely due to the disequilibrium condition of granulite: as granulite is metastable at eclogite facies $P - T$ conditions, any source of energy brought to the system, like a fluid pulse, can instantaneously lead to a fast reaction (Rubie, 1998).

Diffusion coefficients of hydrogen can be used to estimate the diffusivity of water, as in Malvoisin et al. (2020). Diffusivity of hydrogen in granulite and eclogite minerals (clinopyroxene, garnet, feldspar, zoisite) at 650-700 °C is between 10^{-15} and $10^{-11} \text{ m}^2 \cdot \text{s}^{-1}$ (Ingrin and Blanchard, 2006; Farver, 2010). The value we deduced from our numerical model is close to these experimentally determined values and shows that modelling the fluid flow by a diffusion process is reasonable. With a numerical model of Holsnøy eclogite shear zones, Kaatz et al. (2021) determined a value of $D = 10^{-16 \pm 1}$, which is in agreement with our work.

7.7. Model limitations

In reality, the fluid flow is likely to be controlled by fluid pressure and porosity, following Darcy's law (e.g. Connolly and Podladchikov, 1998). The fluid pressure varies when metamorphic reactions consume or release free fluid. The transformation of granulite into eclogite also induces a significant increase in rock density (Austrheim, 1987; Centrella, 2019, this work), which decreases the rock volume, thus increasing the porosity and enhancing the fluid flow. These couplings between metamorphic reactions, fluid flow and pressure variations are complex, and only few numerical models allow an in-depth study of these processes (Malvoisin et al., 2015; Omlin et al., 2017; Schmalholz et al., 2020). Implementing all these couplings in our 1D model is out of the scope of this work. However, our model accurately replicates field and petrological observations, with parameters in good agreement with those found in the literature. Therefore, even if our 1D

numerical model cannot be used as a perfectly quantitative tool, we argue that it provides a sensible insight of the processes at work in the shear zones. A more complex model, with an approach similar to that of Malvoisin et al. (2015) and Schmalholz et al. (2020), would allow to refine the findings of our study.

8. Conclusion

In Holsnøy, field observations suggest that the instantaneous shear is higher on the edge of the eclogite shear zones than in the core. This is consistent with the rheological evolution across a shear zone: away from the shear zone, the granulite is dry and is composed of millimetre-sized grains of strong phases (plagioclase, garnet). In the edge of the shear zone, the foliation is marked by interconnected weak layers of denser and smaller grains, and strong layer inherited from the granulite coronas. In the core of the shear zone, the weak phases are less abundant, the foliation is less pronounced and the grains are larger than in the edge of the shear zone. This suggests that the edge of a shear zone is mechanically weaker than its core. As the shear zones widen over time, this spatial evolution is interpreted as a temporal evolution from the unreacted granulite to the fully reacted eclogite. This suggests that transient weakening occurs in the shear zones of Holsnøy, during the granulite to eclogite metamorphic reaction. The weakening is likely to be caused by a combination of grain size reduction and volume decrease. Textural heterogeneities inherited from the protolith are still present in the transforming rock. Textural and chemical equilibration at the cm- and dm-scale is only reached at the end of the reaction, and triggers the hardening of the eclogite.

Pairing petrological and field investigations with numerical modelling confirms the occurrence of transient weakening. We showed that the widening of the shear zones is not only caused by fluid infiltration, but also by shear zone hardening. We highlight the importance of both the reaction rate and the diffusivity on the evolution of eclogite shear zones.

9. Acknowledgements

This work has been partially supported by the INSU SYSTER program. P.Y. thanks the Institut Universitaire de France for financial support. The authors thank Håkon Austrheim and Torgeir Andersen for their help on the field and for insightful discussions, Thibault Duret for his

help with numerical modelling, and Omar Boudouma and Nicolas Rividi for their assistance on SEM and EPMA analyses. We thank Tim Johnson and an anonymous reviewer for very helpful comments that have improved and clarified the paper. The MATLAB numerical code is available on request to E.B.

Credit statement

Erwan Bras: Software, Conceptualisation, Methodology, Investigation, Visualisation, Writing - Original Draft, Review & Editing. **Marie Baisset:** Conceptualisation, Investigation, Resources, Writing - Review & Editing. **Philippe Yamato:** Conceptualisation, Investigation, Supervision, Writing - Review & Editing. **Loic Labrousse:** Investigation, Supervision, Writing - Review & Editing.

Declaration of interest statement

We confirm that this manuscript has not been published elsewhere and is not under consideration by another journal. All authors have approved the manuscript and agree with submission to Tectonophysics. We have read and have abided by the statement of ethical standards for manuscripts submitted to Tectonophysics. The authors have no conflict of interest to declare.

References

- Abers, G.A., Hacker, B.R., 2016. A matlab toolbox and excel workbook for calculating the densities, seismic wave speeds, and major element composition of minerals and rocks at pressure and temperature. *Geochemistry, Geophysics, Geosystems* 17, 616–624. doi:<https://doi.org/10.1002/2015GC006171>.
- Andersen, T.B., Jamtveit, B., Dewey, J.F., Swenson, E., 1991. Subduction and exhumation of continental crust: Major mechanisms during continent-continent collision and orogenic extensional collapse, a model based on the south norwegian caledonides. *Terra Nova* 3, 303–310. doi:<https://doi.org/10.1111/j.1365-3121.1991.tb00148.x>.
- Austrheim, H., 1987. Eclogitization of lower crustal granulites by fluid migration through shear zones. *Earth and Planetary Science Letters* 81, 221–232. doi:[https://doi.org/10.1016/0012-821X\(87\)90158-0](https://doi.org/10.1016/0012-821X(87)90158-0).
- Austrheim, H., 1990. The granulite-eclogite facies transition: A comparison of experimental work and a natural occurrence in the bergen arcs, western norway. *Lithos* 25, 163–169. doi:[https://doi.org/10.1016/0024-4937\(90\)90012-P](https://doi.org/10.1016/0024-4937(90)90012-P).
- Austrheim, H., 1991. Eclogite formation and dynamics of crustal roots under continental collision zones. *Terra Nova* 3, 492–499.

doi:<https://doi.org/10.1111/j.1365-3121.1991.tb00184.x>.

- Austrheim, H., 1998. Influence of fluid and deformation on metamorphism of the deep crust and consequences for the geodynamics of collision zones, in: Hacker, B.R., Liou, J.G. (Eds.), *When Continents Collide: Geodynamics and Geochemistry of Ultrahigh-Pressure Rocks*. Springer Netherlands, Dordrecht, pp. 297–323. doi:https://doi.org/10.1007/978-94-015-9050-1_12.
- Austrheim, H., 2013. Fluid and deformation induced metamorphic processes around moho beneath continent collision zones: Examples from the exposed root zone of the caledonian mountain belt, w-norway. *Tectonophysics* 609, 620–635. doi:<https://doi.org/10.1016/j.tecto.2013.03.030>.
- Austrheim, H., Griffin, W.L., 1985. Shear deformation and eclogite formation within granulite-facies anorthosites of the bergen arcs, western norway. *Chemical Geology* 50, 267–281. doi:[https://doi.org/10.1016/0009-2541\(85\)90124-x](https://doi.org/10.1016/0009-2541(85)90124-x).
- Bascou, J., Barruol, G., Vauchez, A., Mainprice D., Eglydio-Silva, M., 2001. Ebsd-measured lattice-preferred orientations and seismic properties of eclogites. *Tectonophysics* 342, 61–80. doi:[https://doi.org/10.1016/S0040-1951\(01\)00156-1](https://doi.org/10.1016/S0040-1951(01)00156-1).
- Bascou, J., Tommasi, A., Mainprice D., 2002. Plastic deformation and development of clinopyroxene lattice preferred orientations in eclogites. *Journal of Structural Geology* 24, 1357–1368. doi:[https://doi.org/10.1016/S0191-8141\(01\)00137-7](https://doi.org/10.1016/S0191-8141(01)00137-7).
- Baxter, E.F., 2003. Natural constraints on metamorphic reaction rates. Geological Society, London, Special Publications 220, 183–202. doi:<https://doi.org/10.1144/GSL.SP.2003.220.01.11>.
- Beane, R., Field, C., 2007. Kyanite deformation in whiteschist of the ultrahigh-pressure metamorphic kokchetav massif, kazakhstan. *Journal of Metamorphic Geology* 25, 117–128. doi:<https://doi.org/10.1111/j.1525-1314.2007.00692.x>.
- Bhowany, K., Hand, M., Clark, C., Kelsey, D.E., Reddy, S.M., Pearce, M.A., Tucker, N.M., Morrissey, L.J., 2018. Phase equilibria modelling constraints on p–t conditions during fluid catalysed conversion of granulite to eclogite in the bergen arcs, norway. *Journal of Metamorphic Geology* 36, 315–342. doi:<https://doi.org/10.1111/jmg.12294>.
- Bingen, B., Davis, W.J., Austrheim, H., 2001. Zircon u-pb geochronology in the bergen arc eclogites and their proterozoic protoliths, and implications for the pre-scandian evolution of

- the caledonides in western norway. *Geological Society of America Bulletin* 113, 640–649. doi:[https://doi.org/10.1130/0016-7606\(2001\)113<0640:ZUPGIT>2.0.CO;2](https://doi.org/10.1130/0016-7606(2001)113<0640:ZUPGIT>2.0.CO;2).
- Bjørnerud, M.G., Austrheim, H., Lund, M.G., 2002. Processes leading to eclogitization (densification) of subducted and tectonically buried crust. *Journal of Geophysical Research: Solid Earth* 107, ETG–14. doi:<https://doi.org/10.1029/2001JB000527>.
- Boundy, T.M., Fountain, D.M., Austrheim, H., 1992. Structural development and petrofabrics of eclogite facies shear zones, bergen arcs, western norway: implications for deep crustal deformational processes. *Journal of Metamorphic Geology* 10, 127–146. doi:<https://doi.org/10.1111/j.1525-1314.1992.tb00075.x>.
- Brodholt, J., Wood, B., 1993. Simulations of the structure and thermodynamic properties of water at high pressures and temperatures. *Journal of Geophysical Research: Solid Earth* 98, 519–536. doi:<https://doi.org/10.1029/92JB01407>.
- Brodie, K.H., Rutter, E.H., 1985. On the relationship between deformation and metamorphism, with special reference to the behavior of basic rocks, in: Thompson, A.B., Rubie, D.C. (Eds.), *Metamorphic Reactions: Kinetics, Textures, and Deformation*. Springer New York, New York, NY, pp. 138–179. doi:https://doi.org/10.1007/978-1-4612-5066-1_6.
- Brodie, K.H., Rutter, E.H., 1987. The role of transiently fine-grained reaction products in syntectonic metamorphism: natural and experimental examples. *Canadian Journal of Earth Sciences* 24, 556–564. doi:<https://doi.org/10.1139/e87-054>.
- Centrella, S., 2019. The granulite-to-eclogite-and amphibolite-facies transition: a volume and mass transfer study in the Lindås nappe, bergen arcs, west norway. *Geological Society, London, Special Publications* 478, 241–264. doi:<https://doi.org/10.1144/SP478.9>.
- Chen, S., Hiraga, T., Kohlstedt, D.L., 2006. Water weakening of clinopyroxene in the dislocation creep regime. *Journal of Geophysical Research: Solid Earth* 111. doi:<https://doi.org/10.1029/2005JB003885>.
- Connolly, J.A.D., Podladchikov, Y.Y., 1998. Compaction-driven fluid flow in viscoelastic rock. *Geodinamica Acta* 11, 55–84. doi:[https://doi.org/10.1016/S0985-3111\(98\)80006-5](https://doi.org/10.1016/S0985-3111(98)80006-5).
- Cruz-Uribe, A.M., Feineman, M.D., Zack, T., Barth, M., 2014. Metamorphic reaction rates at 650–800° c from diffusion of niobium in rutile. *Geochimica et Cosmochimica Acta* 130, 63–

77. doi:<https://doi.org/10.1016/j.gca.2013.12.015>.
- Fagereng, Å., Biggs, J., 2019. New perspectives on ‘geological strain rates’ calculated from both naturally deformed and actively deforming rocks. *Journal of Structural Geology* 125, 100–110. doi:<https://doi.org/10.1016/j.jsg.2018.10.004>.
- Farver, J.R., 2010. Oxygen and hydrogen diffusion in minerals. *Reviews in Mineralogy and Geochemistry* 72, 447–507. doi:<https://doi.org/10.2138/rmg.2010.72.10>.
- Fossen, H., Cavalcante, G.C.G., 2017. Shear zones—a review. *Earth-Science Reviews* 171, 434–455. doi:<https://doi.org/10.1016/j.earscirev.2017.05.002>.
- Früh-Green, G.L., 1994. Interdependence of deformation, fluid infiltration and reaction progress recorded in eclogitic metagranitoids (sesia zone, western alps). *Journal of Metamorphic Geology* 12, 327–343. doi:<https://doi.org/10.1111/j.1525-1314.1994.tb00026.x>.
- Glodny, J., Kühn, A., Austrheim, H., 2008. Geochronology of fluid-induced eclogite and amphibolite facies metamorphic reactions in a subduction–collision system, bergen arcs, norway. *Contributions to Mineralogy and Petrology* 156, 27–48. doi:<https://doi.org/10.1007/s00410-007-0272-y>.
- Godard, G., van Roermund, H.L., 1995. Deformation-induced clinopyroxene fabrics from eclogites. *Journal of Structural Geology* 17, 1425–1443. doi:[https://doi.org/10.1016/0191-8141\(95\)00038-F](https://doi.org/10.1016/0191-8141(95)00038-F).
- Goncalves, P., Oliot, E., Marquer, D., Connolly, J., 2012. Role of chemical processes on shear zone formation: an example from the grimsel metagranodiorite (aar massif, central alps). *Journal of Metamorphic Geology* 30, 703–722. doi:<https://doi.org/10.1111/j.1525-1314.2012.00991.x>.
- Gueydan, F., Leroy, Y.M., Jolivet, L., Agard, P., 2003. Analysis of continental midcrustal strain localization induced by microfracturing and reaction-softening. *Journal of Geophysical Research: Solid Earth* 108. doi:<https://doi.org/10.1029/2001JB000611>.
- Handy, M.R., 1989. Deformation regimes and the rheological evolution of fault zones in the lithosphere: the effects of pressure, temperature, grainsize and time. *Tectonophysics* 163, 119–152. doi:[https://doi.org/10.1016/0040-1951\(89\)90122-4](https://doi.org/10.1016/0040-1951(89)90122-4).
- Handy, M.R., 1990. The solid-state flow of polymineralic rocks. *Journal of Geophysical Research: Solid Earth* 95, 8647–8661. doi:<https://doi.org/10.1029/JB095iB06p08647>.

- Handy, M.R., 1994. Flow laws for rocks containing two non-linear viscous phases: a phenomenological approach. *Journal of Structural Geology* 16, 287–301. doi:[https://doi.org/10.1016/0191-8141\(94\)90035-3](https://doi.org/10.1016/0191-8141(94)90035-3).
- Hawemann, F., Mancktelow, N.S., Pennacchioni, G., Wex, S., Camacho, A., 2019. Weak and slow, strong and fast: How shear zones evolve in a dry continental crust (musgrave ranges, central australia). *Journal of Geophysical Research: Solid Earth* 124, 219–240. doi:<https://doi.org/10.1029/2018JB016559>.
- Hetényi, G., Cattin, R., Brunet, F., Bollinger, L., Vergne, J., Nábělek, J.L., Diament, M., 2007. Density distribution of the india plate beneath the tibetan plateau: Geophysical and petrological constraints on the kinetics of lower-crustal eclogitization. *Earth and Planetary Science Letters* 264, 226–244. doi:<https://doi.org/10.1016/j.epsl.2007.09.036>.
- Hirth, G., Teyssier, C., Dunlap, J.W., 2001. An evaluation of quartzite flow laws based on comparisons between experimentally and naturally deformed rocks. *International Journal of Earth Sciences* 90, 77–87. doi:<https://doi.org/10.1007/s005310000152>.
- Huet, B., Yamato, P., Grasemann, B., 2014. The minimized power geometric model: an analytical mixing model for calculating polypphase rock viscosities consistent with experimental data. *Journal of Geophysical Research: Solid Earth* 119, 3897–3924. doi:<https://doi.org/10.1002/2013JB010453>.
- Incel, S., Renner, J., Jamtveit, B., 2020. Evolution of brittle structures in plagioclase-rich rocks at high-pressure and high-temperature conditions—linking laboratory results to field observations. *Geochemistry, Geophysics, Geosystems* 21, e2020GC009028. doi:<https://doi.org/10.1029/2020GC009028>.
- Ingrin, J., Blanchard, M., 2006. Diffusion of hydrogen in minerals. *Reviews in Mineralogy and Geochemistry* 62, 291–320. doi:<https://doi.org/10.2138/rmg.2006.62.13>.
- Jackson, J.A., Austrheim, H., McKenzie, D., Priestley, K., 2004. Metastability, mechanical strength, and the support of mountain belts. *Geology* 32, 625–628. doi:<https://doi.org/10.1130/G20397.1>.
- Jakob, J., Alsaif, M., Corfu, F., Andersen, T.B., 2017. Age and origin of thin discontinuous gneiss sheets in the distal domain of the magma-poor hyperextended pre-caledonian margin of baltica, southern norway. *Journal of the Geological Society* 174, 557–571.

doi:<https://doi.org/10.1144/jgs2016-049>.

Jamtveit, B., Austrheim, H., Putnis, A., 2016. Disequilibrium metamorphism of stressed lithosphere. *Earth-Science Reviews* 154, 1–13.

doi:<https://doi.org/10.1016/j.earscirev.2015.12.002>.

Jamtveit, B., Ben-Zion, Y., Renard, F., Austrheim, H., 2018. Earthquake-induced transformation of the lower crust. *Nature* 556, 487–491.

doi:<https://doi.org/10.1038/s41586-018-0045-y>.

Jamtveit, B., Bucher-Nurminen, K., Austrheim, H., 1990. Fluid controlled eclogitization of granulites in deep crustal shear zones, bergen arcs, western norway. *Contributions to Mineralogy and Petrology* 104, 184–193.

doi:<https://doi.org/10.1007/BF00306442>.

Jamtveit, B., Petley-Ragan, A., Incel, S., Dunkel, K.C., Dupart, C., Austrheim, H., Corfu, F., Menegon, L., Renard, F., 2019. The effects of earthquakes and fluids on the metamorphism of the lower continental crust. *Journal of Geophysical Research: Solid Earth* 124, 7725–7755.

doi:<https://doi.org/10.1029/2018JB016461>.

Jolivet, L., Raimbourg, H., Labrousse, L., Avigad, D., Leroy, Y., Austrheim, H., Andersen, T.B., 2005. Softening triggered by eclogitization, the first step toward exhumation during continental subduction. *Earth and Planetary Science Letters* 237, 532–547.

doi:<https://doi.org/10.1016/j.epsl.2005.06.047>.

Kaatz, L., Zertani, S., Moulas, E., John, T., Labrousse, L., Schmalholz, S.M., Andersen, T.B., 2021. Widening of hydraulic shear zones during incipient eclogitization of metastable dry and rigid lower crust – holsnøy, western norway. *Tectonics*, e2020TC006572

doi:<https://doi.org/10.1029/2020TC006572>.

Klaper, E.M., 1990. Reaction-enhanced formation of eclogite-facies shear zones in granulite-facies anorthosites. *Geological Society, London, Special Publications* 54, 167–173.

doi:<https://doi.org/10.1144/GSL.SP.1990.054.01.16>.

Kohlstedt, D.L., 2006. The role of water in high-temperature rock deformation. *Reviews in mineralogy and geochemistry* 62, 377–396.

doi:<https://doi.org/10.2138/rmg.2006.62.16>.

Koons, P.O., Rubie, D.C., Früh-Green, G., 1987. The effects of disequilibrium and deformation on the mineralogical evolution of quartz diorite during metamorphism in the eclogite facies.

- Journal of Petrology 28, 679–700.
doi:<https://doi.org/10.1093/petrology/28.4.679>.
- Kretz, R., 1983. Symbols for rock-forming minerals. *American mineralogist* 68, 277–279.
- Labrousse, L., Hetényi, G., Raimbourg, H., Jolivet, L., Andersen, T.B., 2010. Initiation of crustal-scale thrusts triggered by metamorphic reactions at depth: Insights from a comparison between the himalayas and scandinavian caledonides. *Tectonics* 29, TC5002.
doi:<https://doi.org/10.1029/2009TC002602>.
- Malvoisin, B., Austrheim, H., Hetényi, G., Reynes, J., Hermann, J., Baumgartner, L.P., Podladchikov, Y.Y., 2020. Sustainable densification of the deep crust. *Geology* 48, 673–677.
doi:<https://doi.org/10.1130/G47201.1>.
- Malvoisin, B., Podladchikov, Y.Y., Vrijmoed, J.C., 2015. Coupling changes in densities and porosity to fluid pressure variations in reactive porous fluid flow: Local thermodynamic equilibrium. *Geochemistry, Geophysics, Geosystems* 16, 4362–4387.
doi:<https://doi.org/10.1002/2015GC006019>.
- Mancktelow, N.S., Pennacchioni, G., 2005. The control of precursor brittle fracture and fluid–rock interaction on the development of single and paired ductile shear zones. *Journal of Structural Geology* 27, 645–661. doi:<https://doi.org/10.1016/j.jsg.2004.12.001>.
- Marti, S., Stünitz, H., Heilbronner, K., Plümpner, O., Kilian, R., 2018. Syn-kinematic hydration reactions, grain size reduction, and dissolution–precipitation creep in experimentally deformed plagioclase–pyroxene mixtures. *Solid Earth* 9, 985–1009.
doi:<https://doi.org/10.5194/se-9-985-2018>.
- Mattey, D., Jackson, D.H., Harris, N.B.W., Kelley, S., 1994. Isotopic constraints on fluid infiltration from an eclogite facies shear zone, holsenøy, norway. *Journal of Metamorphic Geology* 12, 311–325.
doi:<https://doi.org/10.1111/j.1525-1314.1994.tb00025.x>.
- Mørk, M.B.E., 1985. A gabbro to eclogite transition on flemsøy, sunnmøre, western norway. *Chemical geology* 50, 283–310.
doi:[https://doi.org/10.1016/0009-2541\(85\)90125-1](https://doi.org/10.1016/0009-2541(85)90125-1).
- Oliot, E., Goncalves, P., Marquer, D., 2010. Role of plagioclase and reaction softening in a metagranite shear zone at mid-crustal conditions (gotthard massif, swiss central alps). *Journal of Metamorphic Geology* 28, 849–871.

- doi:<https://doi.org/10.1111/j.1525-1314.2010.00897.x>.
- Omlin, S., Malvoisin, B., Podladchikov, Y.Y., 2017. Pore fluid extraction by reactive solitary waves in 3-d. *Geophysical Research Letters* 44, 9267–9275. doi:<https://doi.org/10.1002/2017GL074293>.
- Pennacchioni, G., 2005. Control of the geometry of precursor brittle structures on the type of ductile shear zone in the adamello tonalites, southern alps (italy). *Journal of Structural Geology* 27, 627–644. doi:<https://doi.org/10.1016/j.jsg.2004.11.008>.
- Pennacchioni, G., Mancktelow, N., 2018. Small-scale ductile shear zones: neither extending, nor thickening, nor narrowing. *Earth-Science Reviews* 184, 1–12. doi:<https://doi.org/10.1016/j.earscirev.2018.06.004>.
- Poirier, J.P., 1982. On transformation plasticity. *Journal of Geophysical Research: Solid Earth* 87, 6791–6797. doi:<https://doi.org/10.1029/JB087iB08p06791>.
- Putnis, A., Austrheim, H., 2010. Fluid-induced processes: metasomatism and metamorphism. *Geofluids* 10, 254–269. doi:<https://doi.org/10.1111/j.1468-8123.2010.00285.x>.
- Putnis, A., Jamtveit, B., Austrheim, H., 2017. Metamorphic processes and seismicity: the bergen arcs as a natural laboratory. *Journal of Petrology* 58, 1871–1898. doi:<https://doi.org/10.1093/petrology/egx076>.
- Raimbourg, H., 2005. Mécanismes d'éclogitisation et conséquences pour l'exhumation des roches métamorphiques de haute pression: l'exemple de l'Arc de Bergen, Norvège. Ph.D. thesis. Paris 6.
- Raimbourg, H., Jolivet, L., Labrousse, L., Leroy, Y., Avigad, D., 2005. Kinematics of syneclogite deformation in the bergen arcs, norway: implications for exhumation mechanisms. *Geological Society, London, Special Publications* 243, 175–192. doi:<https://doi.org/10.1144/GSL.SP.2005.243.01.13>.
- Reuss, A., 1929. Berechnung der fließgrenze von mischkristallen auf grund der plastizitätsbedingung für einkristalle. *Zeitschrift für Angewandte Mathematik und Mechanik* 9, 49–58.
- Roberts, D., 2003. The scandinavian caledonides: event chronology, palaeogeographic settings and likely modern analogues. *Tectonophysics* 365, 283–299. doi:[https://doi.org/10.1016/S0040-1951\(03\)00026-X](https://doi.org/10.1016/S0040-1951(03)00026-X).

- Rubie, D.C., 1986. The catalysis of mineral reactions by water and restrictions on the presence of aqueous fluid during metamorphism. *Mineralogical Magazine* 50, 399–415. doi:<https://doi.org/10.1180/minmag.1986.050.357.05>.
- Rubie, D.C., 1990. Mechanisms of reaction-enhanced deformability in minerals and rocks. Springer Netherlands, Dordrecht. pp. 262–295. doi:https://doi.org/10.1007/978-94-011-6827-4_11.
- Rubie, D.C., 1998. Disequilibrium during metamorphism: the role of nucleation kinetics. Geological Society, London, Special Publications 138, 199–214. doi:<https://doi.org/10.1144/GSL.SP.1996.138.01.12>.
- Rutter, E.H., Brodie, K.H., 1988a. Experimental “syntectonic” dehydration of serpentinite under conditions of controlled pore water pressure. *Journal of Geophysical Research: Solid Earth* 93, 4907–4932. doi:<https://doi.org/10.1029/JB093iB05p04907>.
- Rutter, E.H., Brodie, K.H., 1988b. The role of tectonic grain size reduction in the rheological stratification of the lithosphere. *Ceologische Rundschau* 77, 295–307. doi:<https://doi.org/10.1007/BF01048691>.
- Rutter, E.H., Brodie, K.H., 1995. Mechanistic interactions between deformation and metamorphism. *Geological Journal* 30, 227–240. doi:<https://doi.org/10.1002/gj.3350300304>.
- Rybacki, E., Dresen, G., 2000. Dislocation and diffusion creep of synthetic anorthite aggregates. *Journal of Geophysical Research: Solid Earth* 105, 26017–26036. doi:<https://doi.org/10.1029/2000JB900223>.
- Schmalholz, S.M., Mous, E., Plümper, O., Myasnikov, A.V., Podladchikov, Y.Y., 2020. 2d hydro-mechanical-chemical modeling of (de)hydration reactions in deforming heterogeneous rock: The periclase-brucite model reaction. *Geochemistry, Geophysics, Geosystems* 21, e2020GC009351. doi:<https://doi.org/10.1029/2020GC009351>.
- Schneider, J., Bosch, D., Monie, P., Bruguier, O., 2007. Micro-scale element migration during eclogitisation in the bergen arcs (norway): a case study on the role of fluids and deformation. *Lithos* 96, 325–352. doi:<https://doi.org/10.1016/j.lithos.2006.10.001>.
- Shi, F., Wang, Y., Yu, T., Zhu, L., Zhang, J., Wen, J., Gasc, J., Incel, S., Schubnel, A., Li, Z., Chen, T., Liu, W., Prakapenla, V., Jin, Z., 2018. Lower-crustal earthquakes in southern tibet are linked to eclogitization of dry metastable granulite. *Nature communications* 9, 1–13.

doi:<https://doi.org/10.1038/s41467-018-05964-1>.

- Snow, E., Yund, R.A., 1987. The effect of ductile deformation on the kinetics and mechanisms of the aragonite-calcite transformation. *Journal of metamorphic Geology* 5, 141–153. doi:<https://doi.org/10.1111/j.1525-1314.1987.tb00376.x>.
- Steffen, K., Selverstone, J., Brearley, A., 2001. Episodic weakening and strengthening during synmetamorphic deformation in a deep-crustal shear zone in the alps. Geological Society, London, Special Publications 186, 141–156. doi:<https://doi.org/10.1144/GSL.SP.2001.186.01.09>.
- Stünitz, H., Neufeld, K., Heilbronner, R., Finstad, A.K., Konopásek, J., Mackenzie, J.R., 2020. Transformation weakening: Diffusion creep in eclogites as a result of interaction of mineral reactions and deformation. *Journal of Structural Geology* 139, 104129. doi:<https://doi.org/10.1016/j.jsg.2020.104129>.
- Stünitz, H., Tullis, J., 2001. Weakening and strain localization produced by syn-deformational reaction of plagioclase. *International Journal of Earth Sciences* 90, 136–148. doi:<https://doi.org/10.1007/s005310000148>.
- Tullis, J., Yund, R.A., 1980. Hydrolytic weakening of experimentally deformed westerly granite and hale albite rock. *Journal of Structural Geology* 2, 439–451. doi:[https://doi.org/10.1016/0191-8141\(80\)90005-x](https://doi.org/10.1016/0191-8141(80)90005-x).
- Vitale, S., Mazzoli, S., 2008. Heterogeneous shear zone evolution: the role of shear strain hardening/softening. *Journal of Structural Geology* 30, 1383–1395. doi:<https://doi.org/10.1016/j.jsg.2008.07.006>.
- Voigt, W., 1928. *Lehrbuch der kristallphysik*. Teubner, Leipzig, Germany.
- Yund, R.A., Tullis, J., 1991. Compositional changes of minerals associated with dynamic recrystallization. *Contributions to Mineralogy and Petrology* 108, 346–355. doi:<https://doi.org/10.1007/BF00285942>.
- Zertani, S., Labrousse, L., John, T., Andersen, T.B., Tilmann, F., 2019. The interplay of eclogitization and deformation during deep burial of the lower continental crust—a case study from the bergen arcs (western norway). *Tectonics* 38, 898–915. doi:<https://doi.org/10.1029/2018TC005297>.
- Zhang, J., Green II, H.W., Bozhilov, K.N., 2006. Rheology of omphacite at high temperature and pressure and significance of its lattice preferred orientations. *Earth and Planetary Science*

Tables and figures captions

Table 1 caption: Representative EPMA data of minerals in SZ1 (average of representative analyses), given with one sigma standard deviation. Omphacite is normalised to 6 oxygens (O), mica to 11 O, plagioclase to 8 O, garnet to 12 O, zoisite to 12.5 O.

Averaged over	Cpx	Omphacite				Plagioclase			Phe ngite	Grt	Grt core	Grt rim	Zoisite	Averaged over
		D0	D2 cor	D2 mat	D3 cor	D3 mat	D4	D0	D2- D4	D2- D4	D0	D2- D4	D2- D4	
	46.4	54.0	55.2	55.1	55.5	55.5	58.2	65.7	47.4	41.3	40.9	39.5	39.2	
	2±1.	9±1.	7±0.	5±0.	9±0.	2±0.	7±0.	8±0.	3±0.	3±0.	±0.2	4±0.	9±0.	
SiO ₂	32	49	27	42	36	24	45	92	25	48	3	23	3	SiO ₂
	2.13	0.23	0.09			0.08	0.03	0.01	0.33	0.18	0.08	0.06	0.04	
	±1.7	±0.0	±0.0	0.2±	0.1±	±0.0	±0.0	±0.0	±0.1	±0.0	±0.0	±0.0	±0.0	
TiO ₂	6	5	3	0.07	0.06	5	3	2		3	6	4	4	TiO ₂
	13.6	12.7	14.2	12.4	13.9	13.4	27.6	27.0	31.9	23.7	23.1	22.4	32.6	
Al ₂ O ₃	6±0.	2±0.	1±0.	9±0.	5±0.	6±0.	4±0.	2±0.	7±0.	6±0.	7±0.	1±0.	4±0.	Al ₂ O ₃
	4	39	16	59	4	33	4	57	33	35	15	2	58	
	0.01	4.09	3.99	3.38		3.6	0.02	0.08	49.4	0.02	13.4	20.7	1.23	
Cr ₂ O ₃	±0.0	±1.2	±0.1	±0.2	3.9±	±0.1	±0.0	±0.0	8±0.	±0.0	1±0.	1±1.	±0.5	Cr ₂ O ₃
	2	1	6	3	0.17	6	2	6	65	3	98	35	4	
	5.17	0.00	0.00	0.01	0.02	0.02	0.03	0.02	0.01	14.1	0.04	0.02	0.02	
	±0.3	±0.0	±0.0	±0.0	±0.0	±0.0	±0.0	±0.0	±0.0	±0.4	±0.0	±0.0	±0.0	
FeO	2	3	4	2	2	2	4	3	2	9	4	3	2	FeO
	10.5	8.49	6.81	8.58	7.03	7.66	0.00	0.00	2.31	15.4	15.0	8.85	0.02	
	3±0.	±0.0	±0.1	±0.4	±0.1	±0.2	±0.0	±0.0	±0.1	2±0.	2±0.	±1.0	±0.0	
MgO	27	7	6	6	1	4	1	1	4	2	55	4	3	MgO
	0.02	0.04	0.02	0.03	0.05	0.03	0.01	0.02	0.02	0.22	0.19		0.02	
	±0.0	±0.0	±0.0	±0.0	±0.0	±0.0	±0.0	±0.0	±0.0	±0.0	±0.0	0.5±	±0.0	
MnO	4	6	3	3	4	3	2	1	2	7	4	0.14	3	MnO
	20.9	13.7	11.6	14.0	12.0	12.6	8.62	2.87	0.03	7.43	7.68	8.56	23.9	
	7±0.	5±0.	1±0	5±0.	3±0.	2±0.	±0.2	±0.7	±0.0	±0.2	±0.0	±1.2	±0.3	
CaO	88	36	22	81	64	22	5	4	3	2	7	3	8	CaO
	2.35	6.43	7.62	6.53	7.58	7.28	6.64	10.1	0.92	0.03	0.02	0.02	0.03	
	±0.1	±0.2	±0.1	±0.4	±0.3	±0.1	±0.1	7±0.	±0.3	±0.0	±0.0	±0.0	±0.0	
Na ₂ O	2	5	4	4	3	4	7	48	6	3	1	2	2	Na ₂ O
	0.02	0.01	0.00	0.01	0.01	0.01	0.25	0.08		0.03	0.01	0.00	0.01	
	±0.0	±0.0	±0.0	±0.0	±0.0	±0.0	±0.1	±0.0	8.96	±0.0	±0.0	±0.0	±0.0	
K ₂ O	4	1	1	1	2	2	2	7	±0.6	3	1	1	1	K ₂ O
	101.	99.8	99.6	100.	100.	100.	101.	101.	95.4	102.	100.	100.	97.2	
Total	28	3	1	43	24	34	52	06	8	52	51	67	0	Total
Si	1.69	1.93	1.96	1.95	1.96	1.96	2.57	2.87	3.25	2.96	2.97	2.98	3.01	Si
Al	0.59	0.54	0.59	0.52	0.58	0.56	1.44	1.13	2.48	2.01	1.98	1.99	2.95	Al
Mg	0.57	0.45	0.36	0.45	0.37	0.40			0.23	1.65	1.62	0.99		Mg
Fe	0.16	0.12	0.12	0.10	0.12	0.11			0.08	0.84	0.81	1.31	0.08	Fe
Ca	0.82	0.53	0.44	0.53	0.45	0.48	0.41	0.13		0.57	0.60	0.69	1.96	Ca
Na	0.17	0.44	0.52	0.45	0.52	0.50	0.57	0.86	0.12		0.00	0.00		Na

K End- mem bers	Ca- Ts = 0	0.09	0.04	0.06	0.04	0.05	0.01	0.00	0.75	Alm = 0.27	0.27	0.43	K End- mem bers	
	Di = 0.63	0.39	0.32	0.41	0.33	0.36	Ab = 0.57	0.86		Grs = 0.18	0.20	0.23		
	Hd = 0.17	0.11	0.10	0.09	0.10	0.10	An = 0.41	0.13		Prp = 0.54	0.53	0.33		
	Jd = 0.19	0.42	0.54	0.44	0.52	0.50	Kfs = 0.01	0.00						
N	10	4	9	26	9	10	4	9	15	10	5	10	27	N

Table 1 footnote: Cor = coronas. Mat = matrix, including the matrix and the omp+ky assemblages at the matrix/corona or matrix/garnet boundary. All Fe is counted as Fe²⁺. N = number of averaged analyses.

Table 2 caption: Representative EPMA data of minerals in SZ2 (average of representative analyses), given with one sigma standard deviation. Structural formulas and abbreviations as in table 1.

	Cpx	Omphacite			Plagioclase		Phengite		Grt core	Grt rim	Zoisit e	Averag ed over
Averag ed over	D1	D3 cor	D3 mat	D4	D1	D3 + D4	D1	D3 + D4	All	All	All	Averag ed over
SiO ₂	49.64 ±1.77	55.7 4±0.32	55.7 9±0.51	55.0 9±0.27	54.7 4±0.72	65.6 4±0.59	47.7 6±0.3	47.4 9±0.65	40.7 1±0.14	39±0.42	39.1 5±0.31	SiO ₂
TiO ₂	0.89± 0.26	±0.0 4	±0.0 4	±0.0 4	±0.0 1	±0.0 2	±0.1 3	±0.0 7	±0.0 7	±0.0 6	±0.0 1	TiO ₂
Al ₂ O ₃	10.28 ±1.96	14.8 ±0.2	5±0.7	9±0.09	±0.2 8	7±0.32	6±0.41	1±0.67	4±0.2	6±0.27	±0.3 2	Al ₂ O ₃
Cr ₂ O ₃	0.03± 0.03	±0.0 3	±0.0 4	±0.0 2	±0.0 1	±0.0 3	±0.0 3	±0.0 4	±0.0 3	±0.0 3	±0.0 1	Cr ₂ O ₃
FeO	3.49± 0.23	±0.2 9	4.25 ±0.2	±0.1 8	±0.0 1	±0.1 3	±0.1 2	±0.2 1	±0.3 6	7±1.19	1.12 ±0.5	FeO
MgO	12.13 ±0.78	6.2± 0.22	±0.4 9	±0.1 4	±0.0 0	±0.2 1	±0.1 2	±0.2 3	8±0.49	7.54 ±0.9	±0.0 3	MgO
MnO	0.01± 0.01	±0.0 2	±0.0 5	±0.0 4	±0.0 2	±0.0 2	±0.0 3	±0.0 2	±0.0 6	±0.1 3	±0.0 3	MnO
CaO	20.35 ±1.31	9±0.41	1±0.64	2±0.12	±0.4 4	±0.5 8	±0.0 3	±0.0 2	±0.3 5	±0.4 2	8±0.31	CaO
Na ₂ O	2.24±	8.16	8.37	7.61	9.65	10.3	0.34	1.82	0.01	0.05	0.04	Na ₂ O

	0.63	±0.2	±0.4	±0.1	±0.2	2±0.	±0.1	±0.3	±0.0	±0.0	±0.0	
		8		3	4	3	3		1	2	1	
		0.01	0.00	0.00	0.32		10.6	8.53	0.00	0.00	0.00	
K2O	0.03±	±0.0	±0.0	±0.0	±0.0	0.1±	1±0.	±0.3	±0.0	±0.0	±0.0	K2O
	0.04	1	1	1	6	0.08	21	5	1	1	1	
		100.	100.		100.	100.	94.6	94.4	100.	100.	97.2	
Total	99.08	40	24	0.49	10	35	0	4	64	30	0	Total
Si	1.82	1.96	1.96	1.96	2.85	2.88	3.23	3.19	2.99	2.99	3.00	Si
Al	0.44	0.61	0.63	0.59	1.16	1.12	2.50	2.59	1.99	1.99	2.97	Al
Mg	0.66	0.33	0.31	0.36			0.24	0.18	1.47	0.86		Mg
Fe	0.11	0.13	0.13	0.12			0.09	0.08	0.93	1.44	0.07	Fe
Ca	0.80	0.41	0.39	0.44	0.14	0.12			0.62	0.68	1.96	Ca
Na	0.16	0.56	0.57	0.52	0.82	0.88	0.05	0.24				Na
K					0.02	0.01	0.91	0.73				K
End-member					Ab							End-member
s	Ca-Ts				=0.8							s
	= 0.22	0.04	0.04	0.05	3	0.88			0.31	0.48		
	Di =				An =				Gr =			
	0.61	0.28	0.27	0.31	0.15	0.12			0.2	0.22		
	Hd =				Kfs =				Prp =			
	0.1	0.11	0.11	0.11	0.02	0.01			0.48	0.28		
	Jd =											
	0.07	0.57	0.59	0.54								
N	7	8	10	12	3	11	7	11	8	7	4	N

Table 3 caption: Parameters used in the numerical model.

Parameter	Symbol	Unit	Value		
Duration	t	Ma	0.5		
Background strain rate	$\dot{\epsilon}$	s ⁻¹	10 ⁻¹⁴		
Temperature	T	°C	700		
Initial fluid pulse	f ₀	-	50		
Reaction threshold	f _t	-	0.5		
Parameter	Symbol	Unit	Granulite	Reacting granulite	Eclogite
Pre-exponential factor	A	Pa ⁻ⁿ s ⁻¹	5.01 x 10 ⁻¹	6.31 x 10 ⁻³⁶	7.94 x 10 ⁻¹⁸
Exponent	n	-		3	4
Activation energy	Q	kJ.mol ⁻¹		648	135
Viscosity at $\dot{\epsilon} = 10^{-14}$	η	Pa.s	2.47 x 10 ²²		1.06 x 10 ²¹
Concentration of fluid in rock	f	cm ⁻¹		0	0.5
					0.25

Figure 1 caption: Geological map of northern Holsnøy island, in south-western Norway, modified from Austrheim (2013) and Zertani et al. (2019). Inset shows the position of Holsnøy in the Lindås Nappe (blue). Black squares indicate the location of the shear zones studied in this work. Shear zone SZ1: 60°34'57"N, 5°00'43.56"E. Shear zone SZ2: 60°35'20.1"N, 5°00'27.8"E.

Figure 2 caption: Photographs and interpretative sketches of shear zones SZ1 (a, c) and

SZ2 (b, d), showing the location of the samples. SZ1: petrological domains D2, D3 and D4 were sampled in the transect ho19-06. D0 was sampled in the granulite outside the photograph. SZ2: domains D1 (drill cores m18a and m18e), D3 (m18b and m18d) and D4 (m18c) were sampled. See section 4.1 for a description of the domains. Notice how the foliation is more pronounced in the edge of the shear zone than in the core.

Figure 3 caption: Figure 3: Petrological features of the domains D0 (a, b, c), D1 (d, e, f), D2 (g, h, i), D3 (j, k, l) and D4 (m, n, o). Most samples are weakly retrogressed in the amphibolite facies. (a, b, c) Detail of a thin section (a), photomicrograph (b) and SEM image (c) showing a typical granulite texture of coarse clinopyroxenes and garnets in a plagioclase matrix. The plagioclase is locally clouded by zoisite needles. (d) Typical granulite texture of coarse clinopyroxenes and garnets in a $Ab+Zo+Ky+Ph+Qtz$ matrix. (e) Photomicrograph showing exsolution lamellae of garnet in clinopyroxene in a corona (left) and reaction rims between garnet/clinopyroxene and the $Ab+Zo+Ky+Ph+Qtz$ matrix. The structure of former coarse plagioclase grains is still visible in the matrix. (f) Phase map derived from EDS element maps. The matrix is made up of Ab, Zo and minor $Ky\pm Ph\pm Qtz$. The reaction rim comprises $Omp+Zo+Ab+Ky+Ph$. (g, h) Contact between a corona ($Omp+Grt+Ph$) and the matrix ($Ab+Zo+Ky+Ph+Qtz$), with an $Omp+Ky$ assemblage at the corona/matrix boundary. The foliation is more pronounced than in D1. (i) Phase map of the matrix showing the foliation. (j) The foliation is well defined by $Omp+Ky$ and $Zo+Ky+Qtz+Ph$ beds. The coronas are more elongated than in D2. (k, l) Reaction rim of Omp, Ky at the garnet/matrix boundary. (m, n, o) Homogeneous $Omp+Ky+Zo+Grt+Ph\pm Qtz$ eclogite assemblage.

Figure 4 caption: Estimated volumetric proportions of peak minerals in SZ1 and SZ2. Minor phases and retrograde minerals are not included. Proportions below 5 % are not labelled.

Figure 5 caption: Schematic diagram illustrating the spatial and temporal evolution of a metre-scale eclogite shear zone. From left to right, the sequence of diagrams shows both the spatial evolution of eclogitisation from the border to the core of a shear zone as observed on the field (D0 to D4), as well as the inferred temporal evolution of granulite from the start (t_0) to the end of the eclogitisation (t_4). Dots and dashes indicate the foliation, denser dashes indicating a well pronounced foliation. Blue arrows indicate fluid transport due to dehydration reactions and fluid transport from the centre of the shear zone. Stacked graphs illustrate the changes in mineral abundance due to the metamorphic reactions. The reactions are those described in section 5.1,

simplified to only show major minerals. Mineral proportions are qualitative.

Figure 6 caption: Numerical model setup. (a) Initial state of the model. A finite amount of fluid is injected in a narrow band of width $H = 5$ cm, which mimics the initial pulse of fluid through a fracture. Simple shear deformation is applied at the top boundary. (b) Changes in viscosity and constitutive fluid content in rock as the reaction progresses from unreacted granulite ($r = 0$) to eclogite ($r = 1$). The evolution of viscosity follows the MPG model of Huet et al. (2014), and the evolution of fluid content follows equation (6).

Figure 7 caption: Final state of a modelled shear zone after $t = 0.5$ Ma, using $D/\dot{\epsilon} = 1$, $\alpha_r/\dot{\epsilon} = 10$, and other parameters as in table 3. (a) Progress of the metamorphic reaction along the vertical profile. (b) Fluid content and viscosity. (c) Geometry and petrology of the shear zone. Granulite is defined by $r < 0.05$, reacting granulite by $0.05 \leq r < 1$, and eclogite by $r = 1$.

Figure 8 caption: Role of D and α_r on (a) the width of the shear zone and (b) the width of the eclogite shear zone core, normalised to the shear zone width. 0.1 means 10 % of the width of the shear zone fully reacted to eclogite, i.e. reached $r = 1$. Contour lines delimit realistic models, with shear zone width between 0.2 and 1 m and normalised eclogite width between 0.1 and 0.9. (c) Shear zone profile of 4 models localised on (a) and (b).

Figure 9 caption: Role of reacting granulite and eclogite strength, relative to granulite strength, on (a) the width of the shear zone and (b) the width of the fully transformed shear zone core, normalised to the shear zone width. In (a), the red domain ($W \approx 0.65$ m) corresponds to a domain where transient weakening occurs: $\eta_t < \eta_g$ and $\eta_t < \eta_e$. The orange domain ($W \approx 0.40$ m) corresponds to a domain of gradual weakening: $\eta_g > \eta_t > \eta_e$. The blue domain ($W \approx 0.20$ m) corresponds to a domain of "transient strengthening": $\eta_t > \eta_g$ and $\eta_t > \eta_e$.

Figure 10 caption: Role of transient weakening on shear zone width. Both cases use the parameters and rheology described in Table 3. (a): changes in viscosity as the reaction progresses from granulite ($r = 0$) to eclogite ($r = 1$). Starting granulite strength and ending eclogite strength are the same in both cases. (b): shear zone geometry. In case A the shear zone is 44 cm wide, and in case B, 62 cm wide. (c): strain rate in the shear zone at two different time steps (middle and end of the simulation) for cases A and B. Without transient weakening the strain rate is localised in the core of the shear zone, whereas it is localised on the edge of the shear zone in the case of transient weakening.

Highlights

- We present a detailed petrological description of the granulite to eclogite reactions.
- We highlight the importance of a transient weakening of the rock during the transformation.
- Shear zone widening is caused by a combination of fluid flow and shear zone hardening.
- Values for fluid diffusivity and metamorphic reaction rate have been estimated using numerical simulations.

Journal Pre-proof

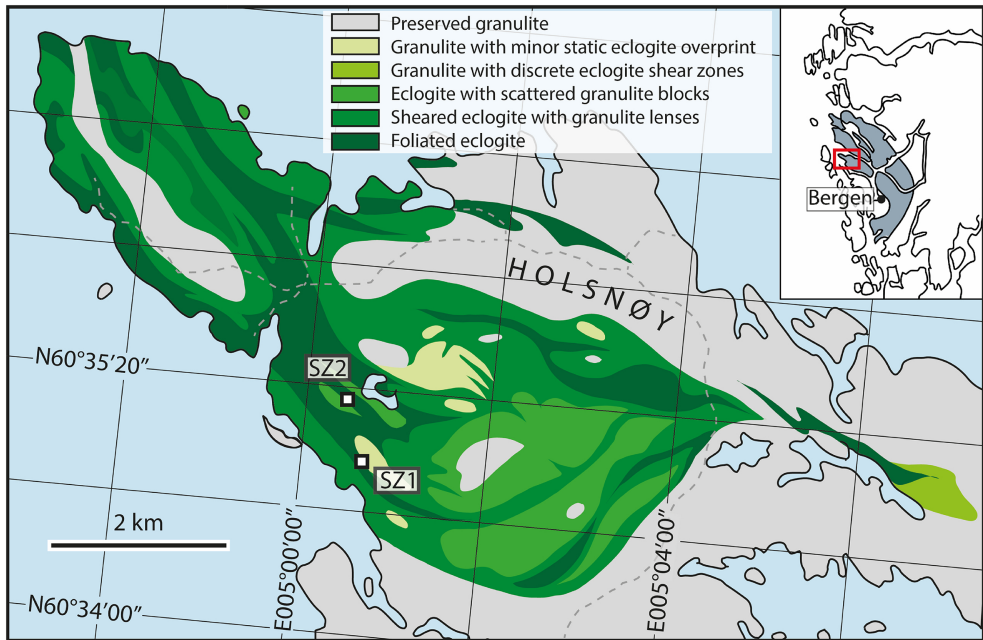


Figure 1

SZ1

SZ2

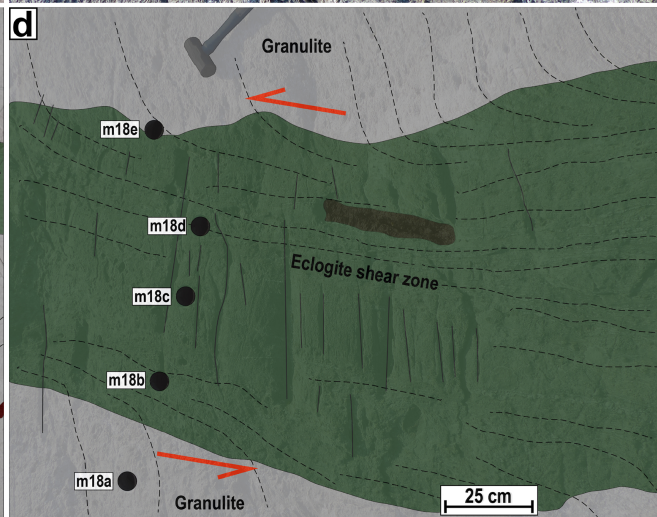
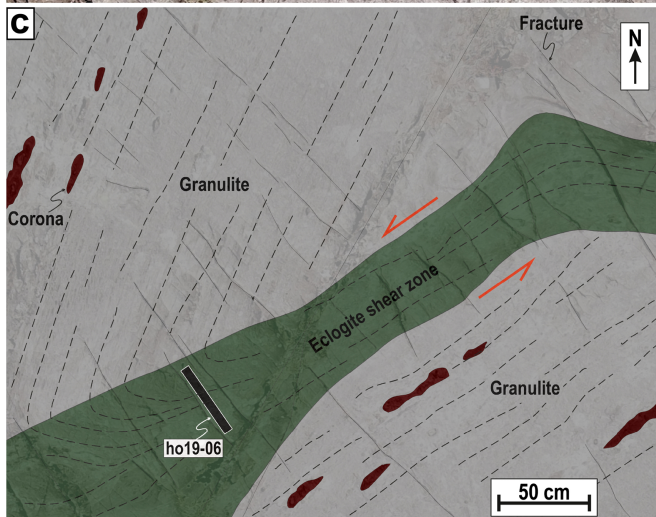
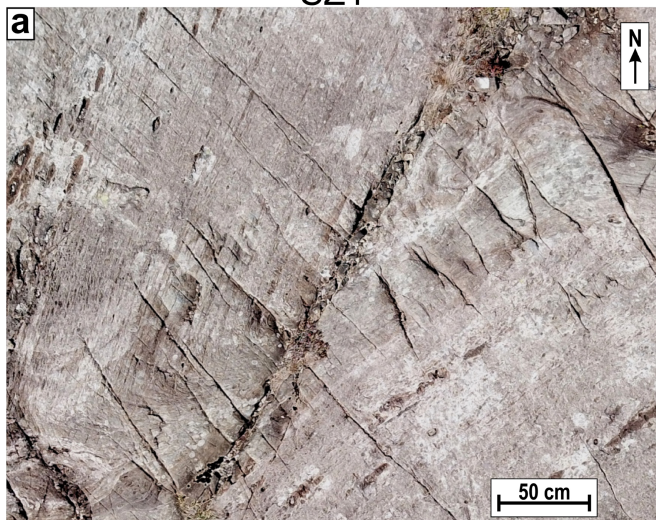


Figure 2

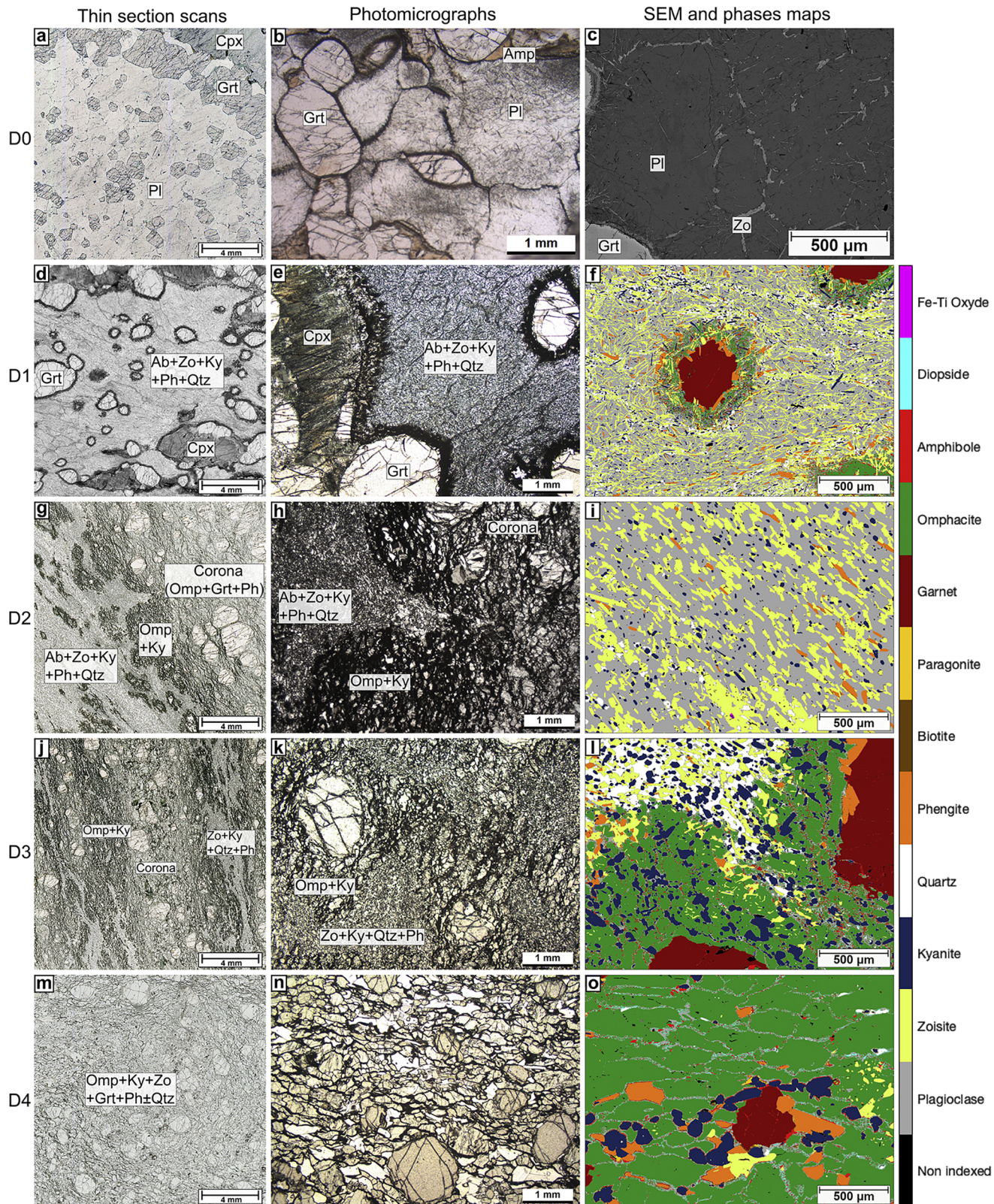


Figure 3

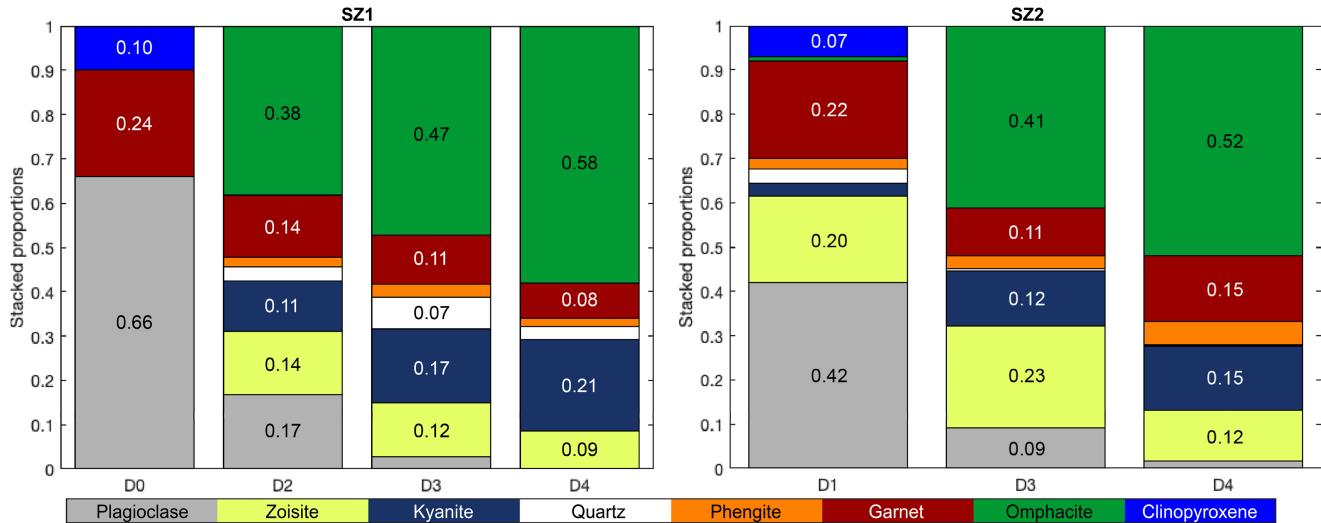


Figure 4

Eclogitisation across a shear zone (D0 → D4) = Eclogitisation through time (t0 → t4)

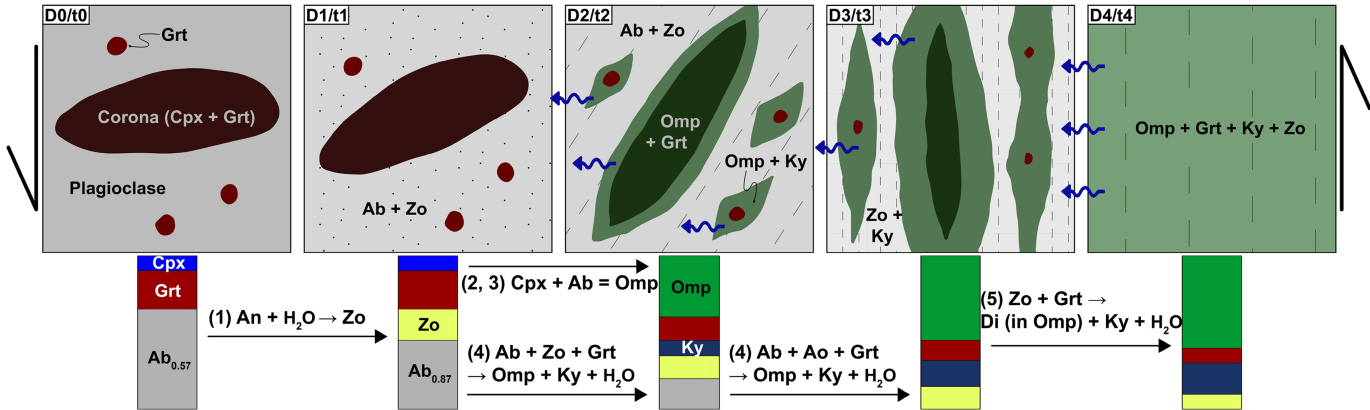


Figure 5

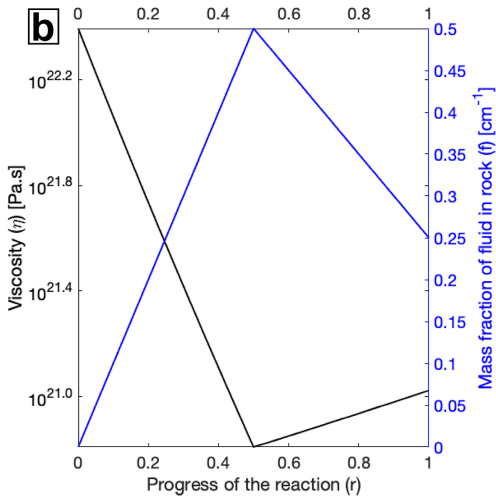
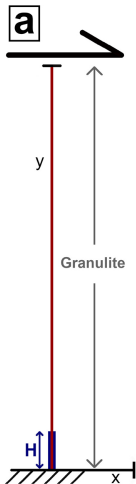


Figure 6

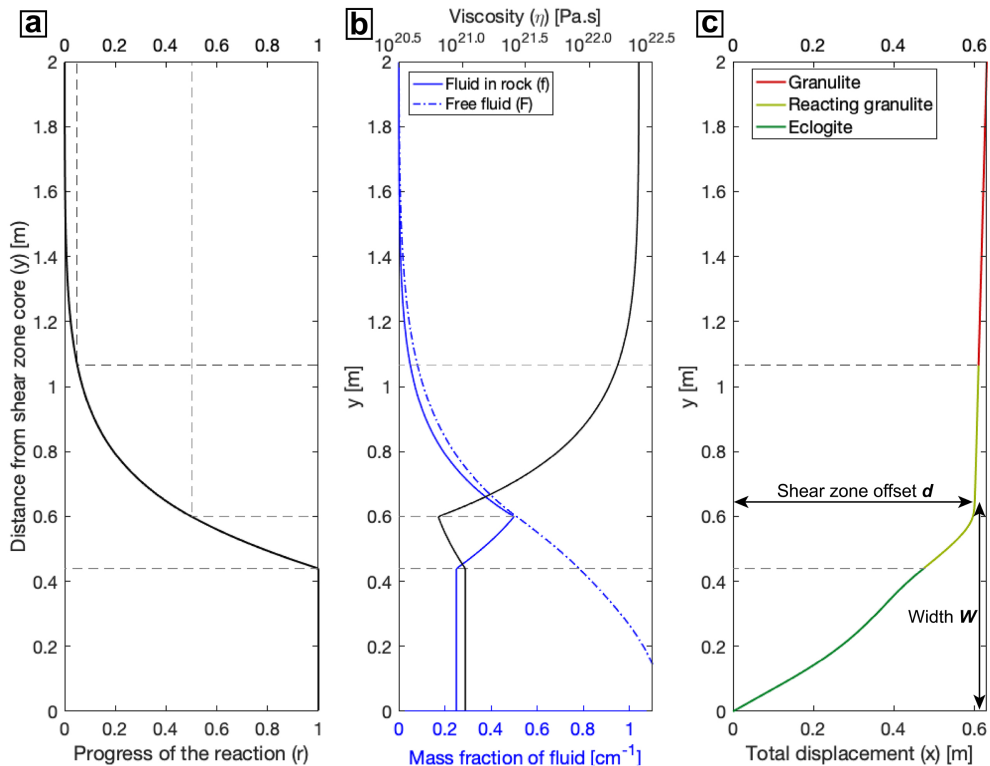


Figure 7

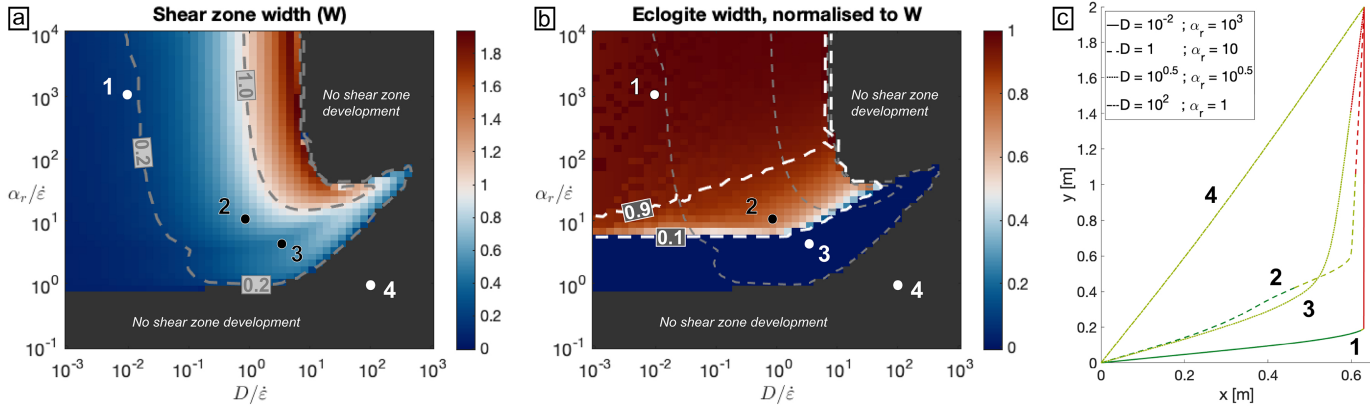


Figure 8

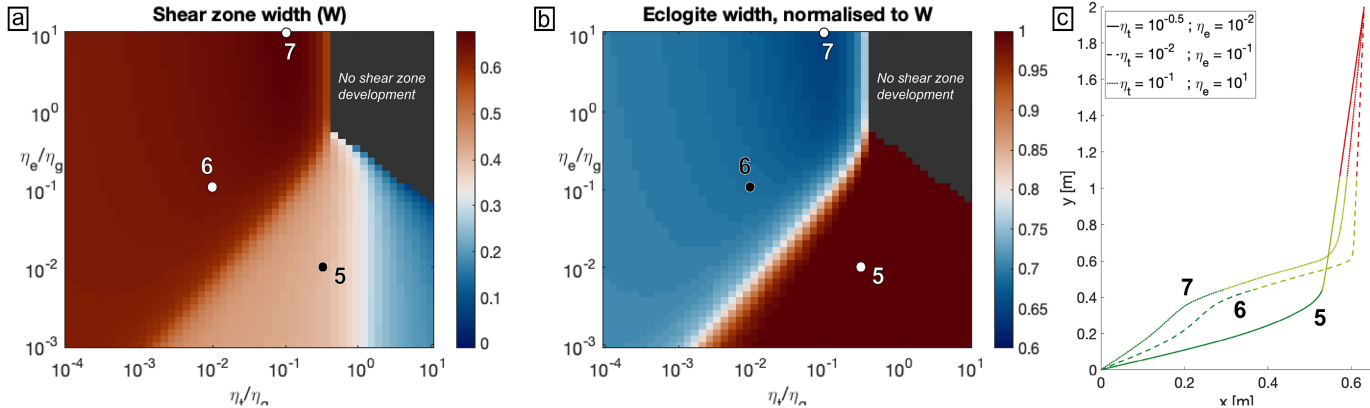


Figure 9

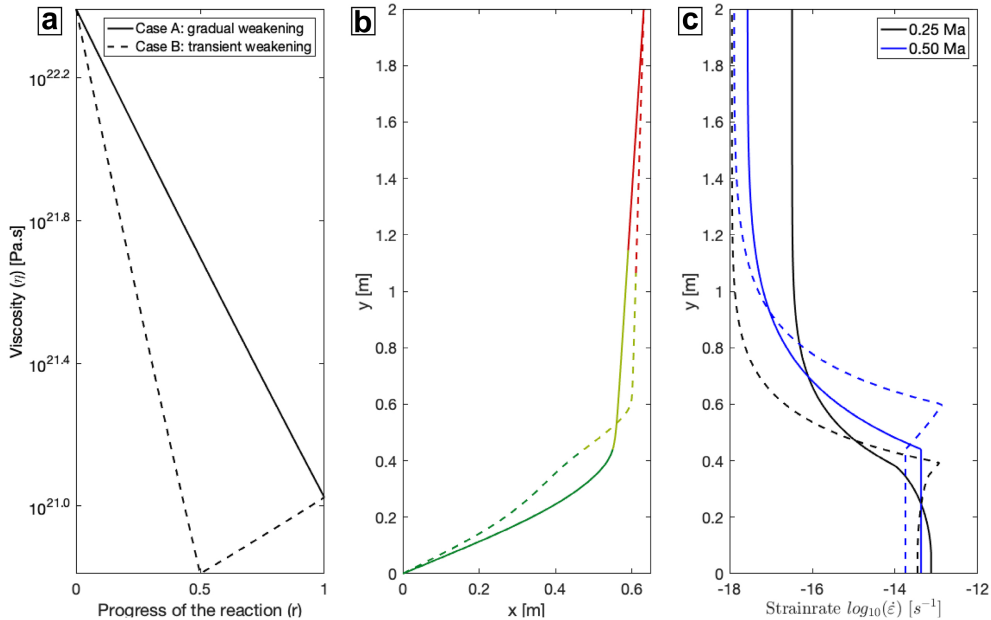


Figure 10